Spectroscopy and Microscopy of Eco-friendly Polymer Composites

Ashish K. Shukla, Chandni Sharma, Syed M. S. Abidi and Amitabha Acharya

List of Abbreviations

AFM	Atomic force microscopy
AT	Nano-Attapulgite
BC	Bacterial cellulose
CASN	Citric acid modified starch nanoparticle
CD	Circular dichroism
CdS QD	Cadium sulfide quantum dot
CHNS	Carbon-hydrogen-nitrogen-sulfur
CNCs	Cellulose nanocrystals
CNS	Cellulose Nanosphere
CPC	Cetylpyridinium chloride
CT/CG	Chitin/cashew gum
DLS	Dynamic light scattering
DMC	Dry-milled corn
DSC	Differential scanning calorimetery
DTPA	Diethylenetriaminepentaacetic acid
EDS	Energy dispersive X-ray spectroscopy
EFPNC	Eco-friendly polymer nanocompositess
FCNTs	Functionalized Carbon nanotube
FESEM	Field emission scanning electron microscope
FTIR	Fourier-transform infrared spectroscopy
GA	Gum arabic
GO	Graphene oxide
HA	Hyaluronan
HRTEM	High resolution transmission electron microscope

A. K. Shukla · C. Sharma · S. M. S. Abidi · A. Acharya (✉)
Biotechnology Division, CSIR-Institute of Himalayan Bioresource Technology,
Palampur 176061, Himachal Pradesh, India
e-mail: amitabha@ihbt.res.in

A. K. Shukla · C. Sharma · S. M. S. Abidi · A. Acharya
Academy of Scientific & Innovative Research (AcSIR), CSIR- Institute of Himalayan
Bioresource Technology, Palampur 176061, Himachal Pradesh, India

Inamuddin et al. (eds.), *Sustainable Polymer Composites and Nanocomposites*,
https://doi.org/10.1007/978-3-030-05399-4_4

ICP-MS	Inductive coupled plasma mass spectroscopy
kDa	Kilodalton
LOX	Lipoxygenase
MCC	Microcrystalline cellulose
MPa	Megapascal
MPTMS	3-(trimethoxysilyl)-propyl methacrylate
NDs	Nanodiamonds
NF	Nanofibrils
NMR	Nuclear magnetic resonance
NPs	Nanoparticles
PBAT	Poly(butylene adipate-co-terephthalate)
PCL	Poly-caprolactone
PDDF	Pair distance distribution function
PGA	Poly-glycolite
PHA	Polyhydroxyalkanoate
PHBV	(3-hydroxybutyrate-co-3-hydroxyvalerate)
PLA	Polylactic acid
PLGA	Poly(D,L-lactide-co-glycolide)
PVA	Polyvinyl alcohol
RChi	Regenerated chitin
SAXS	Small angle X-ray scattering
SCC	Spherical cellulose container
SEM	Scanning electron microscopy
SLRP	Sequential liquid-lignin recovery and purification
SPI/CNTs	Soy protein isolate-carbon nanotube
SPI–MMT	Soy protein isolate–montmorillonite
SPIONs	Superparamagnetic iron oxide
TEM	Transmission electron microscopy
Tg	Glass-rubber transition
TGA	Thermogravimetric analysis
TG-MS	Thermogravimetric-Mass Spectroscopy
Tm	Melting point
UP	Unsaturated polyester
UV-Vis	Ultraviolet-visible spectroscopy
XRD	X-ray diffraction

1 Introduction

The eco-friendly polymers which are also known as green polymers comprise the materials which are either biodegradable or derived from biobased renewable sources. Therefore, these polymers and their corresponding composites trim down the negative human footprint on the environment. In the current scenario, due to the growing environmental issues; it is indeed necessary to put together the great importance for developing “green materials” in both R&D as well as in industries [1]. Photosynthetic components extracted from plants and wood biomass; such as starch, cellulose, hemicellulose, lignin produced from atmospheric carbon dioxide, can be used as renewable carbon resources [2]. Based on the concept of “carbon neutrality”; when biodegradable polymers such as polylactic acid (PLA), polyhydroxyalkanoate (PHA), polysaccharide derivatives are burnt, they are considered as green materials, because the liberated carbon dioxide is again transformed into biomass [3].

NCs are known as the materials of the 21st century; having a unique design and different properties which are lacking in conventional composites [4]. A number of biodegradable polymers and their layered silicate NCs are widely being used for different applications. NCs, as the term indicates are the composites in which at least one of the dimensions falls under nanometre range (1–100 nm). NCs consist of one or more discontinuous phases which are distributed over single continuous phase. The continuous phase is known as matrix whereas discontinuous phase as reinforcing material. Mechanically, NCs are having high aspect ratio and high surface to volume ratio of the reinforcing material. Green composites are made from both renewable sources based on biopolymers and biofillers (including nano-type fillers), with a positive environmental impact.

NCs are the alternative materials for overcoming the lacunae of microcomposites and monolithic; however, NCs may go through the formulation challenges related to the control of elemental composition in nanocluster. NCs possess multifunctional advantages due to some unique properties like smaller filler size, improved ductility with the same strength, light transmission characteristics, flame retardancy, thermal stability and chemical resistance. Three different techniques are usually followed to prepare eco-friendly polymer NCs (EFPNC) which include solution casting, in situ polymerization, and melt processing. Additionally, as dimension reaches the nanometre level, interactions at phase interfaces improved significantly, and this is important to enhance the properties of the material [1].

Polymers which are used as NCs can be classified based on their (a) native biomass such as plants, animals, microbial and synthetic based and (b) chemical structure (polysaccharide and polypeptide based). Eco-friendly polymers can be extracted from the natural sources mainly by chemical treatment and mechanical method including grinding, milling, sonication, and ultrasonication. The prepared polymer NCs are very useful in making lightweight sensors, producing structural components with a high strength to weight ratio, aerospace, automotive, electronics, biotech, and pharmaceutical industries [3].

2 Isolation of Eco-friendly Polymers

This part of the chapter briefly describes different processes used for the isolation of eco-friendly polymers from their natural sources. The described eco-friendly polymers were classified according to their origin viz., plant, animal, microbial and synthetic based (Scheme 1).

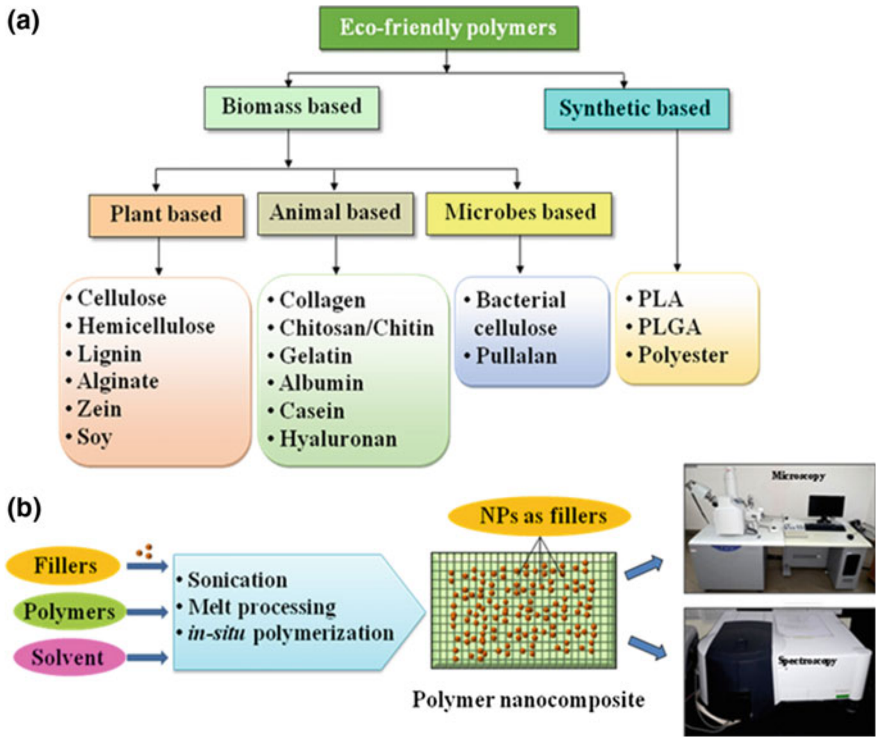

Scheme 1 **a** Pictorial representation of different eco-friendly polymers classified according to their source. **b** Schematic representation of different components of polymer nanocomposites and their characterization techniques

2.1 Eco-friendly Polymers of Plant Origin

Plant-based polymers have gained tremendous attention in recent years due to their high sustainability. In the next section, attempts have been made to concisely report different extraction techniques available in the literature for isolation of plant-based biopolymers.

2.1.1 Cellulose Extraction

Cellulose, with $\sim 10^{11}$ tons of annual turnover, is the most abundant natural polymer, containing vital skeletal polysaccharide component, composed of the β(1–4) glycosidic bond [5]. The biosynthesis of cellulose takes place not only in the plant but also in bacteria viz. Acetobacter, Acanthamoeba, Achromobacter and fungi [6, 7]. Cellulose is an extensive linear-chain polymer with a large number of hydroxy groups (three per anhydroglucose unit). Cellulose from its natural precursor sources can be isolated in two stages. The first stage involves pretreatment of raw material for purification and homogenization depending on the source material and desired morphology of cellulose particles. The pretreatments for plant biomass involve the complete or partial removal of matrix materials (hemicellulose, lignin etc.) and the isolation of individual complete fibers. Detailed descriptions of several of these pretreatment methods are already available in literature [8, 9]. The plant cellulose extraction methods include chemical and mechanical treatment as well as a combination of both. The chemical treatment involves acid hydrolysis [8, 10, 11] whereas the mechanical treatment includes high pressure homogenization [12, 13], grinding, cryo-crushing [14] and sonication [15]. Appropriate treatment of cellulose fibers leads to increase in the inner surface, alters degree of crystallinity, breaks hydrogen bonding and increases the reactivity of the cellulose to further facilitate the process of nanocellulose formation [10].

2.1.2 Hemicellulose Extraction

The hemicelluloses usually comprise off 20–30% of the dry weight of wood. It is the monomer of mixed sugar of short polymer length, consist mainly of mannose along with xylose, glucose, galactose and arabinose, where the main chain is connected to β(1–4) glycosidic bonds. The presence of hydroxyl group on the backbone of hemicellulose creates an opportunity for the chemical modification and can lead to the development of new nanobiocomposite. Lignin content was removed from plant biomass using concentrated NaOH and ethanol, and the resulting holocellulose solids were then extracted using NaOH (10%) to provide a filterate rich in hemicellulose. After the addition of ethanol, the precipitates were collected which predominantly contain xylose based hemicellulose [16, 17].

2.1.3 Lignin Extraction

Lignin is one of the abundant biopolymers after cellulose which is derived from plants and their wastes [18] and acts as connecting bridge between cellulose and hemicellulose. Lignin with cellulose combines to form large lignocellulosic biomass which has a high potential for production of biomaterials and chemicals [18–20]. Lignin can be isolated via different techniques viz., physical and chemical pretreatments and oxidation [21], enzymatic cellulose hydrolysis [22], acidification of black liquors (liquid-lignin) through sequential liquid lignin recovery process (SLRP) [23], pre-hydrolysis using kraft pulping [24] and microwave-assisted acidolysis [25]. Lignin has also been isolated from reed straw via thermomechanical process through attritor-type laboratory ball mill [26].

2.1.4 Starch Extraction

Starch is one of the major dietary sources of carbohydrates and it is found abundantly in the form of polysaccharide in plants. This is an important polymer, formed from long chains of α-glucose units joined together by glycosidic linkages containing two types of molecules i.e. amylose and amylopectin [27]. It is commonly found in roots, tubers, cereal grains and also occurs in a variety of foods, fruits and vegetable tissues etc. Starch and its derivatives have been used as capping and reducing agents for the synthesis of many metallic nanoparticles [28]. Starch is mostly isolated from white rice through alkali extraction method [27]. Acid hydrolysis at 37 °C was used to extract starch from peas to form pea starch nanocomposite [29]. Similarly, starch nanocrystals were also prepared from native pea granules through acid hydrolysis using mild stirring [30]. Enzymatic treatment of waxy maize through α-amylase hydrolysis was also one of the approaches used for starch isolation [31]. Few other techniques include ultrasonication [32], combined enzymatic hydrolysis couple with chemical or physical treatment and acidic treatment was also used for starch isolation [33, 34].

2.1.5 Alginate Extraction

Alginate is the derivative of alginic acid widely distributed in the cell wall of brown algae in the form of calcium, magnesium and sodium salt of alginic acid. These are anionic linear polysaccharides containing β-D mannuronic and α-L-guluronic acid residues linked by β 1–4 glycosidic bond forming homo- and heteropolymeric structures. Alginate biopolymer and its NCs are biocompatible and inexpensive which allows them to be used for various biomedical applications [35]. Alginate extraction was done using broken seaweed pieces, which was then stirred with a hot solution of an alkali, usually sodium carbonate. Alginate nanocomposite can be prepared in a two-step procedure based on the ionotropic pre-gelation of polyanion with calcium chloride salt followed by polycationic crosslinking [36].

2.1.6 Zein Extraction

Maize, a major cereal grain throughout the world, is being used for the isolation of zein. Zein is a protein that is exclusively found in corn. However, there are some other proteins with similar prolamin characteristics, which can be isolated from common cereals such as wheat, barley, rye, and sorghum [37]. Zein extractions require a complex balance between yield, quality, and purity. Dry-milled corn (DMC), acts as a good material to extract zein. Wet milling of corns can also be used to create a co-product that is rich in zein [38].

2.1.7 Soy Extraction

The consumption of soy has gained popularity in the world during recent decades due to (i) increased awareness of the consumer, (ii) drive for a healthier lifestyle, (iii) predominance of lactose intolerance cases and (iv) improved processing of soybeans with reduced off-flavors. Common process of soy extraction steps involves soaking of the soybeans, followed by grinding of the materials in cold water. Subsequently, these materials were then filtered and cooked at 100 °C for 30 min. This method can be further modified by grinding the soy extracts in hot water, which has the advantage of lipoxygenase (LOX) inactivation in the final extract [39].

2.2 Animal-Based Eco-friendly Polymers

This section includes different biopolymers isolated from animal origin viz., collagen, gelatin, chitin and chitosan, casein and hyaluronan.

2.2.1 Collagen Extraction

Collagen is a fibrous protein which is predominantly present in the connective tissues of animals. It offers a wide range of applications in the food, pharmaceuticals, cosmeceuticals and photographic industries. Before the extraction of collagen, a pretreatment is performed using an acid or alkaline process which depends on the origin of the raw material. Collagen can be extracted by both chemical and enzymatic hydrolysis process. Although, chemical hydrolysis is frequently used in many industries, enzymatic hydrolysis shows more potential in obtaining products having high nutritional significance and improved functionality. Furthermore, the enzymatic processes require less processing time and have the advantage of minimal waste generation [40].

2.2.2 Gelatin Extraction

Gelatin is a fibrous denatured polymer derived from collagen protein. It is an important biodegradable polymer having a broad range of applications in food and pharmaceutical industries. Due to its inherent cross-linking property, it has been widely used for nanoparticle synthesis [41]. There are mainly two types of gelatin viz., Type A and Type B which can be obtained via acid and base treatment [42] respectively in combination with thermomechanical process [43].

2.2.3 Chitin Extraction

Chitin is the second most abundant naturally occurring polysaccharide after cellulose and mostly found in crustaceous shell or in cell walls of fungi. Chitin is consisted of repeated homopolymeric β(1→4) linked *N*-acetyl-D-glucosamine units [44]. It has limited industrial application due to its insolubility in commonly used solvents. Further, the isolation of pure chitin from natural sources is difficult. The general methodologies for isolation of chitin involves three main processes viz., demineralization, decolourisation followed by deacetylation. After initial washing and drying, the raw scales were soaked in HCl (1%) solution for 36 h. These were then washed, dried in oven and kept in NaOH (2N) solution for 36 h to complete demineralization. Finally, these scales were immersed in potassium permanganate solution for 1 h, followed by addition of oxalic acid to achieve decolorization. Chitin isolated from the above process was further subjected to NaOH treatment (50% w/v) to obtain deacetylated chitin [45].

2.2.4 Casein Extraction

Casein is an essential protein which approximately counts for 80% of the total protein content of cow milk. Casein is also termed as globular protein, because it generally forms globules in the milk, and is mainly responsible for white color of the milk. Casein in its native form exists as calcium salt, hence termed as calcium caseinate. Casein can be extracted from reconstituted nonfat powdered milk using acetic acid treatment. This procedure allows the extraction of casein in the form of precipitated mass [46].

2.2.5 Hyaluronan (HA) Extraction

HA is a high-molecular-weight unsulfated polysaccharide. HA is mainly composed of subunits of D-glucuronic acid and *N*-acetyl glucosamine which is coupled by β(1–3) and β(1–4) glycosidic linkages. High water-retention capacity, mucoadhesion property, viscoelasticity, non-immunogenicity and biocompatibility make it an ideal candidate for healthcare applications [47]. HA can be obtained from various animal sources, such as umbilical cords, rooster combs, bovine submaxillary glands and zones of maturing chondrocytes. Muscle and skeleton comprises off ~35% of human HA. Extraction procedure of HA mainly includes dissection of bigeye tuna, followed by repeated thawing and filtration of vitreous at 4 °C to isolate the carbohydrate content which was further precipitated by adding cetylpyridinium chloride (CPC) to the filtrate. The HA-CPC complex was separated by re-suspending the precipitated mass in sodium chloride solution followed by centrifugation. Using a series of continued chemical followed by centrifugation process HA was finally isolated as freeze-dried material [48].

2.3 Bacterial-Based Eco-friendly Polymers

2.3.1 Bacterial Cellulose Extraction

Bacterial cellulose shares almost identical chemical structure as that of plant-derived cellulose, though it possesses high degree of polymerization, purity, crystallinity, water holding capacity compared to the later one [49]. This interesting biopolymer has been widely used in food, pharma, paper industry etc. [50]. For the successful production and isolation of BC, several factors such as physiological and nutritional conditions, temperature, incubation time, agitation etc. plays an important role. Standard static condition of bacterial growth is required for the isolation of bacterial cellulose. Glycerol improved the dry mass production of bacterial cellulose approximately 2–3 times as compared to when mannitol and glycerol in combination was used as carbon source [51].

2.3.2 Pullulan Extraction

Pullulan is an extracellular hydrophilic polysaccharide produced by different strains of yeast-like fungus e.g., *Aureobasidium pullulans*. It is synthesized intracellularly at the cell wall and secreted out to the cell surface to form a loose and slimy layer. It comprises of mixed linear linkage of α-D-glucan which consist mainly maltotriose units coupled by α-(1→6) linkages [52]. Pullulanase, is an enzyme belonging to the α-amylase family, identified as glycoside hydrolase and breaks α-(1→6) linkages present in various biopolymers like pullulan, starch and amylopectin [53]. Extraction of pullulan involves the use of fermenter; in which production medium was inoculated with 10% seed culture. Finally, the fermentation was performed at an optimized temperature (27 °C) and air flow condition under optimized revolution ($\sim$210 rpm) for one week to isolate pullulan [52].

2.4 Synthetic Eco-friendly Polymers

2.4.1 PLA Synthesis

PLA is a synthetic biodegradable polymer of lactic acid with two optically active stereoisomers viz., L(+) and D(−). Isolation of lactic acid in industry is mainly accomplished by fermentation process using bacterial strains of *Lactobacillus* genus viz., *Lactobacillus delbrueckii, L. amylophilus, L. bulgaricus and L. leichmanii* at a pH range between 5.4–6.4 and temperature range of 38–42 °C. PLA can be subsequently produced from lactic acid through polymerization process [54].

2.4.2 PLGA Synthesis

Poly(D,L-lactide-co-glycolide) (PLGA) is amongst the most widely used FDA approved biodegradable polymer for bio-applications since it produces metabolite monomers lactic acid and glycolic acid, after its hydrolysis. This copolymer can be synthesized by treating D, L-lactide and glycolide at 175 °C in the presence of stannous octoate and lauryl alcohol. PLGA-nanoparticles are internalized in cells partly through fluid phase pinocytosis and also through clathrin-mediated endocytosis process [55, 56].

2.4.3 Polyesters Synthesis

Polyesters are a class of polymers which can be synthesized as a result of polycondensation (step-growth polymerization) reaction between dialcohol and diacid/ or diester. Unsaturated polyester (UP) resin is widely used in various industrial applications such as marine, automotive, coatings, storage tanks, piping and construction [57].

3 Spectroscopic and Microscopic Characterization of Biopolymers and Their NCs

This part of the chapter includes different spectroscopic and microscopic techniques which were used for the characterization of the described eco-friendly polymers and their corresponding NCs. For the ease of understanding, the discussion in this section was classified based on the chemical structure of the polymers viz., polysaccharide, polypeptide and synthetic based materials.

3.1 Polysaccharide-Based Biopolymers

Polysaccharide-based biopolymers are composed of long chains of monosaccharide units, which are connected by glycosidic bonds. Polysaccharide NCs have become increasingly important materials over the past decade, since these offer a green alternative to synthetic polymers. These have also been used as composites with hard nanomaterials, such as metal nanoparticles and carbon-based nanomaterials (Fig. 1).

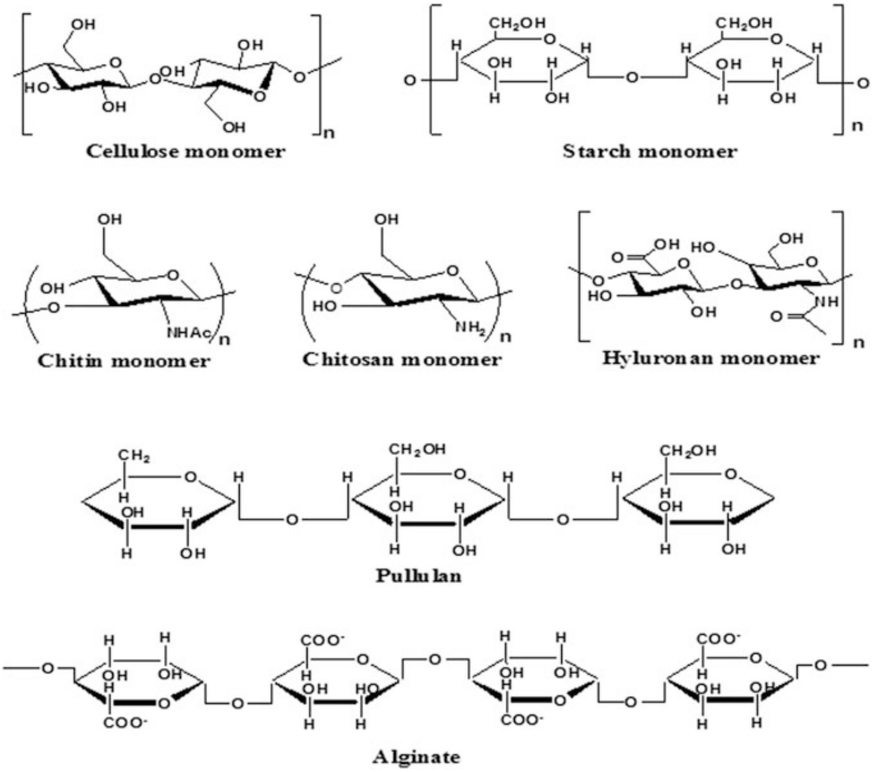

Fig. 1 Chemical structures of different polysaccharide based biopolymers

3.1.1 CHNS Analysis

The elemental analysis of lignin suggested that organosolv and kraft lignin have higher percentage of carbon and lower percentage of nitrogen content compared to other sources of lignin. However, the nitrogen content was higher for aminated lignin of epoxy resin polymer [58]. It was also reported that corn straw and wheat straw contains approximately equal amount carbon, hydrogen, nitrogen, and sulfur [59]. CHNS analysis of modified nanocrystalline cellulose (CNC) revealed higher amount of carbon content and less amount of sulphur and oxygen content as compared to native CNC [60].

3.1.2 FT-IR Spectroscopy

FT-IR has been one of the most common spectroscopic techniques that were used for the identification of different chemical functional groups present in the biopolymers. Numerous studies were already performed on natural fibers by FT-IR

[61]. The peak observed at 3349 cm^{-1} represents the stretching vibration of O–H, related to hydroxyl groups present in lignin, hemicelluloses and cellulose [10]. The C–H stretching vibrations in cellulose, hemicelluloses and lignin were identified at the spectrum range of ~2900 cm^{-1}. The transmittance peak observed at ~1645 cm^{-1} was attributed to the O–H bending vibration which resulted from the interaction between cellulose and the absorbed water molecules [62]. The peak position at ~1462 cm^{-1} present in the spectrum was attributed to the symmetric bending of $–CH_2$ present in sugar backbone whereas the peak at ~1313 cm^{-1} was due to the existence of bending vibration from C–H and C–O bonds in the polysaccharide aromatic rings of cellulose. The peaks observed at ~1216 cm^{-1} and 1157 cm^{-1} were assigned to C–O–C of arylalkyl ether present in lignin and C–H rocking vibration, respectively. The characteristic anhydroglucose chains showed peak at ~1047 cm^{-1} due to C–O stretching. Further, the peak at ~898 cm^{-1} was identified as C–H glycosidic deformation or β-glycosidic linkage and was also known as the amorphous band [10]. Spiridonov et al. [63] reported decrease in –COO– peak in presence of Fe^{3+} coordination for maghemite carboxymethylcellulose NCs. Further, FT-IR studies were also used to evaluate cellulose stability for TiO_2-cellulose nanocomposite prepared by microwave solvothermal process [64]. In another report, a hemicellulose-diethylenetriaminepentaacetic acid (DTPA)-chitosan nanocomposite was characterized by FT-IR studies. The corresponding spectra showed new peaks at ~3030 and 2780 cm^{-1} which indicated the carboxylic acids present in DTPA [65]. The FT-IR spectra of bacterial cellulose almost correspond to the peaks already mentioned for other cellulose species [66]. Foong et al. [67] reported appearance of new IR peaks at ~1720 and 1449 cm^{-1} which corresponds to acetyl and CH_3 groups of PLA and indicated conjugation of PLA on bacterial cellulose surface. A mixed nanocomposite of chitosan and alginate nanoparticles was prepared in presence of glutaraldehyde and characterized using FT-IR. The bands obtained at ~3360–3440 cm^{-1} were assigned as N–H and O–H stretching modes of vibrations for chitosan/alginate NCs. Further, the broadening of IR band confirmed the formation of intermolecular hydrogen bonding for chitosan/alginate NCs [68]. FT-IR spectroscopic analysis of chitin/chitosan revealed that the absorption bands of chitosan were similar to those for standard chitin. IR bands observed in the range of ~3425–2881 cm^{-1} were assigned to N–H stretching for primary amines whereas the bands at ~3425–3422 cm^{-1} were indicative of different vibrations of N–H, O–H and NH_2, present in chitin. When chitin undergoes deacetylation, a higher intensity peak was observed at ~1597 cm^{-1} which suggested effective deacetylation and prevalence of NH_2 group [45]. The chitin and chitosan isolated from *Fusarium solani* present in marine soil revealed the presence of amide I region (~1657–1642 cm^{-1}), amide II stretching with C–O group (~1560–1550 cm^{-1}) and amide III region (1381–1375 cm^{-1}) [69]. The herbal nanocomposite of chitosan showed IR peaks of lower intensity at ~3474/3468 cm^{-1} and 1745/1654 cm^{-1}, possibly due to the presence of intermolecular hydrogen bonding between chitosan and corresponding active ingredients [70]. Pullulan nanocomposite prepared using lysozyme nanofibres (LNF) and polysaccharide solutions were characterized by FT-IR and showed characteristic bands for

both the reactants [71]. The existence of both α-(1→4) and α-(1→6) glycosidic linkages in the pullulan structure was confirmed by the presence of IR band at 935 cm^{-1} [72]. Chemometric analysis of lignin isolated from different sources was also studied using infrared spectroscopy [73]. Although there are various sources of lignin or lignocellulosic biomass, the best quality material can be screened by monitoring characteristic FT-IR spectra [74, 75]. IR peaks at ~800, 1350, 1540 and 3300–3500 cm^{-1} were assigned for N–H vibration, C–N vibration, N–H bending vibration, and N–H stretching vibration of aminated lignin respectively. Further, the peak at ~3400 cm^{-1} was assigned for O–H stretching of demethylated lignin [58] while the peak at ~1270 cm^{-1} was designated for aromatic ring vibration of guaiacyl lignin [74, 76].

Similarly, FT-IR spectra were used for the chemical characterization of corn starch, starch nanoparticles (SN) and citric acid modified starch nanoparticles (CASN). The key difference between CASN compared to corn starch and SN was the appearance of a new peak at ~1738 cm^{-1} for an ester group and at ~1017 cm^{-1} for C–O bond stretching of the C–O–C group of the anhydroglucose ring which was exclusively present in CASN. It was being inferred that in corn starch and SN, the oxygen of the C–O–C group could form the hydrogen-bond with the hydroxyl groups and the ester bonds in CASN, shifting C–O bond stretching of the C–O–C group to 1026 cm^{-1} [77].

3.1.3 Powder XRD

Powder XRD technique has been used widely for the identification of crystalline and amorphous nature of the concerned polymers and their composites. The XRD was used to investigate the crystalline structure of the raw fibers, mercerized cellulose, and CNS. It was observed that the XRD patterns of raw fibers and commercial cellulose were clearly different compared to the mercerized cellulose and cellulose nanoparticles. For the raw fibers, a characteristic 2θ band between 13° (101), 17° (101) along with a broad peak at 22.5° (002) were observed, which corresponds to the cellulose-I structure. These results were in agreement with those observed for native cellulose [78]. It was also observed that the peaks for the amorphous region at 14° and 16° were hard to distinguish due to their close proximity [79]. Further, it was found that in case of mercerized cellulose and CNS, the corresponding peaks were shifted to 12°, 20°, and 22° and were related to same crystal planes mentioned earlier. The crystallinity index for raw material, mercerized cellulose and CNS were found to be ~68, 64 and 88%, respectively [80]. In case of $\mathrm{TiO_2}$–cellulose nanocomposite additional peaks at 34.3° (004), 38.2° (004), 48.0° (200) and 70.11° (220) were observed corresponding to the tetragonal structure of $\mathrm{TiO_2}$ and reflected no change in the crystalline structure of the wood cellulose fibers [64]. Observation of a broad peak at 19° in powder XRD indicated the conversion of hemicellulose to xylitol [81]. Xylan hemicellulose (XH)/cellulose fiber NCs showed the presence of crystalline peaks whereas freeze-dried XH powder showed no distinct crystalline peaks [82]. Bacterial cellulose showed three characteristic peaks of cellulose at 2θ = 14.7° [39], 16.4° [39] and 22.6° (200) which were attributed to the elementary cellulose crystalline structure. Carbon sources used for bacterial growth can also affect the degree of crystallinity in bacterial cellulose. Further, the crystallinity of bacterial cellulose produced in agitated condition was found to be lower than the static culture due to the presence of structural disorder [83]. XRD studies of the bacterial cellulose (BC) and drug-loaded BC matrices were carried out by varying the scanning angle in the range of 10° to 60°. The distinct peaks observed in the diffractogram for BC at 14.12°, 16.8°, and 22.72° demonstrated the crystalline structure of BC. The surface modified BC showed peak pattern similar to as-synthesized BC with lower intensity, indicating a reduction in the crystallinity as a result of acetylation. Apart from the peaks at 26.90°, 28.54° and 29.82°, BC-famotidine matrices have strong peaks at 11.58° and 17.76°, confirming the entrapment of drug into matrices. The appearance of distinct peaks in the pattern for BC-tizanidine matrices at 25.06° and 26.46° showed lower crystal growth of the drug nanocomposite [84]. XRD patterns of calcium alginate/graphene oxide NCs revealed an amorphous structure, whereas those of barium alginate/graphene oxide composites indicated the presence of semi-crystalline structure which might have resulted from the preferential binding of barium ions to mannuronic acid blocks [85]. The XRD patterns of chitin and hydrolyzed chitosan confirmed that all chitin samples exhibited strong reflections at a 2θ value between 9 and 10°. XRD spectra further suggested that chitin is amorphous in nature whereas chitosan is crystalline [45]. Chitin/cashew gum (CT/CG) nanocomposite showed sharp peaks at 2θ = 9.28° and 17.54° corresponding to diffractions of CT and CG segments respectively when blended with metal oxide nanoparticles. Furthermore, peaks at 2θ corresponding to 21.65° and 26.13°, indicated the semi-crystalline nature of the blend matrix [86]. The XRD patterns of carbonized lignin showed peaks at 26.7° (002), 43.2° (100/101), 54.7° (004) and 78.1° (110) confirming the structural changes happened in lignin after carbonization whereas untreated lignin did not show above-mentioned peaks, which revealed its non-crystalline nature [87]. Pure pullulan has no crystalline peaks implying that the material is fully amorphous [88]. Unfilled glycerol plasticized and non-plasticized pullulan films were characterized by a broad peak centered at around 19°, typical of fully amorphous materials [89]. Rice starch showed A-type diffraction pattern peaks at a 2θ value of 9.9°, 15.0°, 17.0°, 18.1° and 23.5°. Extensive hydrolysis of rice starch showed less intensity diffraction patterns which indicated that hydrolysis occurred in the amorphous region [31]. A native starch granule was pre-treated with β-amylase and glucoamylase and found that pretreated starch granules have semi-crystalline nature as compared to native starch [33].

3.1.4 NMR

NMR is a one of the strongest technique which is used for characterization of chemical moiety present in most of the compounds. Microcrystalline cellulose (MCC) biopolymer was converted into spherical cellulose container (SCC) by the sonochemical method and investigated by ^{13}C MAS NMR. The spectra depicted that peak of different carbon atoms of the glucose pyranose repeating unit in MCC and SCC were quite similar [90]. ^{1}H-NMR spectra of acetylated and demethylated lignin showed peaks corresponding to 6.0 and 8.0 ppm for two of its important aromatic precursor's viz., syringyl and guaiacyl respectively. Further, the peak at 6.96 ppm was assigned for a proton of C5 position in the 9 carbon units of lignin while 3.82 ppm peak was designated for a proton of methoxy group of the same material [91]. ^{13}C NMR spectrum of the aminated lignin was observed and showed a peak around 130 ppm which corresponds to ortho- and para- positions of the aromatic ring. Further, peaks were observed at δ value 16.5, 17.8, 59.5, 82.2, 136.8 and 137.3 ppm for methyl groups, CH group of the aromatic ring and amine, CH connected to oxygen and amine connected aromatic carbon atoms respectively [58]. 2D NMR analysis of mild wood lignin showed typical lignin substructures such as β-O-4, β-β, β-5, benzaldehyde and cinnamaldehyde units [92]. ^{31}P NMR is a powerful tool for hydroxyl group analysis in lignin biomass. Softwood lignin showed characteristic peaks of hydroxyl groups present in an aromatic moiety of lignin [93].

3.1.5 DLS and Zeta Potential

The stability of CNS is mainly related to the ions present during the acid hydrolysis. For sulfuric acid treatment, the formation of sulfate ester groups allows water dispersion of CNSs and prevents aggregation. The zeta potential of 0.1% CNS in water indicated an average zeta potential of −23.3 ± 3.2 mV [94]. The DLS size of CNSs was found to be in the broad range 30 nm to 1 μm which indicated the anisotropic properties of the CNS suspension which were attributed to the different aggregate states CNSs in solution [95]. Similarly, for hemicellulose broad particle size distribution ranging from 50 to 400 nm was observed. Further, hemicellulose showed negative zeta potential value which can be due to the presence of pectic substances (anionic polysaccharides) and oxidized lignin structure on hemicellulose surface [96]. Silver-chitosan nanocomposite showed particle diameter of ~1553 nm whereas, simple chitosan showed the diameter of 78.8 nm. The zeta potential analysis of silver chitosan nanocomposite revealed that the prepared nanocomposite was negatively charged (−3.4 mV at neutral pH) [97]. Zeta potential and particle size of chitin nanocomposite was found to increase as the amount of chitin (wt%) were enhanced in the corresponding NCs [98]. The hydrodynamic diameter of magnetic nanoparticles coated by a series of carboxymethylated polysaccharides, such as dextran, cellulose, and pullulan was found to be 229, 719, and 330 nm, respectively. The ζ potential in all of these cases had slightly negative values, which increased with increasing magnetite content present in the composite [99].

3.1.6 UV-Vis

The formation of gold-carboxymethylcellulose (CMC) NCs was confirmed by UV-Vis spectroscopy by monitoring the appearance of Au surface plasmon band at 522 nm which was otherwise absent in case of both the precursors [100]. The absorption intensity of Au was found to gradually increase with increasing CMC concentrations in NCs. Moreover, absorption peak width became narrower suggesting uniform size distribution of synthesized Au nanoparticles in presence of carboxymethyl cellulose [101]. The absorption peak of chitosan ZnO nanocomposite was observed at 360 nm, which was having lesser intensity than macrocrystalline ZnO absorption found at 372 nm. This was attributed to the quantum size effect of chitosan-ZnO nanoparticles [102].

3.1.7 SAXS

SAXS was used to determine pair distances distribution function (PDDF) profile related to the shape and the conformational arrangement of macromolecules. The PDDF profile of the CNS before sonication (CNS-BS) and after sonication (CNS-AS) showed different geometries. Interestingly, the non-sonicated CNS exhibited an elongated curve due to agglomerated particles, whereas the CNS-AS exhibited a Gaussian curve corresponding to spherical particles [103].

3.1.8 TGA

TGA was used to characterize the thermal behaviour of raw fibers, mercerized cellulose and CNS and the values were found to be dependent on components present in the plant cell wall. In fact, the cellulose decomposition was reported in the range of 315–400 °C whereas for hemicellulose and lignin it was found to be between 200–315 °C and 160–900 °C respectively [104]. For the raw fiber, mercerized cellulose and CNS, decomposition started at 218, 223 and 209 °C and the maximum degradation was observed at 346, 342 and 326 °C respectively. It was found that compared to the CNS, the thermal stability of raw fibers and mercerized cellulose was higher, possibly because of the presence of sulfate group at the surface of the CNS. The difference in thermal behaviour between mercerized cellulose and raw fibers was explained based on the presence of hemicellulose and lignin material in the raw fibers [105]. Further, it was found that TiO_2–cellulose nanocomposite was more stable than pure cellulose [64]. Xylan-rich hemicellulose (XH) and cellulose nanocomposite showed good thermal stability than freeze-dried XH powder because of the presence of crystal structure [82]. Further, hemicellulose Fe_3O_4 hydrogel NCs were also studied using TGA [106]. Similarly, bacterial cellulose and its NCs were also evaluated for their thermal stability using TGA studies and found that it resembles quite well with the thermal properties of the plant cellulose. Literature reports suggested that the presence of mineral phase has changed the thermal degradation profiles of the bimetallic–alginate nanocomposite samples when compared with the non-mineralized composite. This might have resulted from the presence of mineral phase which improved the thermal stability of the NCs by lowering the rate of alginate decomposition [107]. TGA thermogram of AgCl/chitin nanocomposite suggested a reduction in the area under endothermic peak in DSC and weight loss in TGA; thus confirming better stability for NCs [108]. The aminated lignins were studied in detail to evaluate their thermal stability [58]. TGA curves for freeze-dried raw starch samples suggested that the maximum loss of mass happened around 260–330 °C and for the same composite, it was noticed at ~300 °C [32].

3.1.9 TGMS

Thermogravimetric- mass spectroscopy (TGMS) has been used to understand the pyrolysis mechanism for hemicellulose. Under inert atmosphere and elevated temperature condition carbonaceous material undergo aromatization. The decomposition of the hemicellulose was observed between 200 and 580 °C and the mass spectroscopy (MS) result showed peaks for CO_2 (m/z = 44), CO (m/z = 28), CH_4 (m/z = 16), and H_2O (m/z = 18) [109].

3.1.10 DSC

DSC is one of the best analytical techniques to find the polymer crystallinity. The same technique can also be used to study oxidation reaction as well as other chemical reactions. DSC thermogram of chitosan-alginate (CS-AL) NCs prepared with glutaraldehyde showed one broad endothermic peak at ~112.1 °C for crystallization temperature whereas the glass transition temperature was found to be ~350 °C. The studies suggested that the crosslinker increases the thermal stability of the corresponding NCs [110]. In a different study, glass-rubber transition (T_g), melting point (T_m), and the degree of crystallinity for the synthetic poly (caprolactone) (PCL) was found to be around ~60, 69 °C, and 58%, respectively. For the developed chitin whiskers/PCL composites, it was found that both T_g and T_m was almost independent of the whiskers concentration [111]. Thermal analysis of developed lignin-epoxy resin suggested enthalpy values were directly proportional to the amine content present in the composites [58]. Further, it was also observed that the enthalpy values of lignin may vary depending on their biomass [18].

3.1.11 ICP-MS

Inductive coupled plasma mass spectroscopy is used to determine the concentration of metallic nanoparticles absorbed on the surface of the nanocomposite. In case of silver/cellulose NCs, prepared by different concentration of silver nitrate in presence of α-cellulose, carboxymethyl cellulose and amino-cellulose as stabilizers, showed that the quantity of silver nanocluster present on cellulose sample was directly proportional to the concentration of silver nitrate in the precursor solution [112].

3.1.12 SEM

SEM was used to understand the surface morphology of raw fibers before and after each treatment for cellulose extraction. The morphology of the fibers changed due to the purification process. In general, the raw fibers are constituted by bundles of cellulose microfibrils and are covered by different layers. The structural morphology of microfibrils cannot be visualized, as they are still buried inside lignin and hemicellulose [113]. For mercerized cellulose, the surface was found to be more clean, smooth and the available microfibrils can be clearly seen. Thus, SEM characterization clearly distinct between raw fibers and the mercerized cellulose. Similarly, CNSs obtained after the acid hydrolysis showed a narrow size distribution of particle size in the range of 46 ± 17 nm. SEM image revealed the three-dimensional structure of hemicellulose/chitosan nanocomposite having continuous cell pore structure [106]. Similarly, the SEM studies on BC showed structure composed of a random network of cellulose nanofibers. It was reported that the outer surface consists of dense layers covering an internal microstructure in the shape of honeycombs whereas the inner region is composed of fibers forming large pores [114]. SEM images of the alginate-zinc oxide NCs appeared to be rough which may have resulted from the interaction between the nanoparticles and the alginate matrix. The presence of ZnO-NPs in the alginate matrix was observed as bright spots with a moderate degree of agglomeration. The presence of elemental Zn was also confirmed by EDS analysis. [115]. The diameter of chitin nanowhisker determined by SEM was found to be much higher compared to the actual whiskers diameter. This resulted from a charge concentration effect due to the emergence of chitin whiskers [116]. Drug-loaded pullulan films appeared to have a random distribution of drug particles with no sign of complete phase separation, thus indicating a nanocomposite structure in the films [117]. Carbon microparticles derived from lignin were analyzed using SEM and the data were compared with untreated lignin, thermo-stabilised lignin and carbonized lignin. The average particle size for untreated, thermostabilised and carbonized lignin was found to be 9.1, 7.0 and 5.3 μm respectively [87]. SEM analysis of dilute acid pretreated corn stover revealed the formation of semispherical and spherical structures on its surface which led to the hypothesis that the droplet formations evolved from the lignocellulosic matrix of corn stover during pre-acid treatment [118]. The microstructures of maize, mango, and banana starch granules were observed by SEM imaging. Mango starch granules were found to be spherical and domeshaped with some non-uniform growth and spoting having 5–10 μm particles size, which clearly indicated that the starch particles may have collapsed during drying. In case of maize and starch granules, regular spherical shaped particles were observed. Banana starch granules were elongated and lenticular in shape, and the average longitudinal dimension was found to be 40 μm with a radius around 20 μm [34]. Citric acid modified starch nanoparticles (CASN) and native starch nanoparticles (SN) was found to have a size range between 50–100 nm and 50–300 nm respectively [77]. In one of the reports, the fractured structure of lamella indicated the homogenous dispersity of SN on soy protein matrix [30].

3.1.13 TEM

In TEM, CNS samples showed mainly the presence of aggregates created during the slow drying process [119]. Interestingly, white regions were observed inside the particles and have been related to the entanglement or local twist of the crystalline regions [120]. TEM studies were performed for alginate-ZnO nanocomposite to monitor size, morphology and dispersion of ZnO NPs on the nanocomposite. It was observed that the polymer conjugated ZnO NPs represented an irregular spherical shape with size variations between 20 and 100 nm which was almost comparable to the bare ZnO NPs [115]. Interfacial adhesion between lignin nanoparticles and PVA matrix was observed through TEM. Lignin nanoparticles showed no change in aggregation states even after incorporation of PVA matrix which suggested an interaction of lignin hydroxyl groups with PVA [121]. The TEM images of superparamagnetic nanoparticles coated by pullalan revealed that the average size for all of the samples varied between 3.4 and 9 nm depending on the amount of magnetite present in the nanocomposite [99]. TEM image of chitosan-ZnO NCs revealed that the particles possess mostly rod-like structure with a size close to 100 nm [102]. HRTEM studies were also used for such characterization [86]. TEM images of pea starch nanoparticles suggested aggregated NPs having a length of ~60–150 nm and width of 15–30 nm [30]. Another report suggested the formation of well dispersed and spherical shaped starch colloids of sizes ~200 nm [32].

3.1.14 AFM

AFM is an imaging technique used for characterizing the surface topology of solid materials. AFM based morphological studies reflected the existence of absorbed nanoparticles on the surface of hemicellulose NCs [96]. Films formed by xylan hemicellulose and chitosan showed a very smooth surface with few nodules. Studies further suggested that cellulose nanofilm have higher roughness factor as compared to cellulose nanofibers [82, 122]. AFM images of GO-alginate biopolymer suggested an average thickness of the sheets was about 1.0 nm, which indicated the formation of single-layered exfoliated GO for the nanocomposite [123]. AFM has been directly applied for the surface analysis of lignin and its polymer composites. The AFM images of hydrothermally pretreated wheat straw and corn stover revealed that the parenchyma cell lining has an aggregate of cellulose fibers and the integrity of microfibers remained intact. The AFM images of pullalan nanocomposite of magnetite nanoparticles revealed that the magnetite nanoparticles had a strong tendency to form agglomerate in the dry state. The magnetite nanoparticles were found uniformly distributed throughout the samples; whereas the aggregation was observed at a higher concentration of magnetite [99]. The AFM images of cross-linked chitosan/chitin NCs showed well isolated nanometer-scale crystals of chitin. The diameter of chitin nanocrystals was found to vary between 13 and 20 nm [124]. In another literature report, the homogeneity of regenerated chitin (RChi) films was investigated by AFM [125].

3.2 Polypeptide-Based Biopolymers

Peptides are emerging as a new class of biomaterials due to their unique chemical, physical, and biological properties. The development of peptide-based biomaterials is driven by the convergence of protein engineering and macromolecular self-assembly. The next section focuses on different spectroscopic and microscopic techniques used for characterization of polypeptide-based polymers (Fig. 2).

3.2.1 CHNS Analysis

Elemental analysis of the collagen waste from goat skins revealed the % of C, N, H and S to be approximately 41.5, 14.7, 7.1 and 0.2%, respectively. Further, XPS and

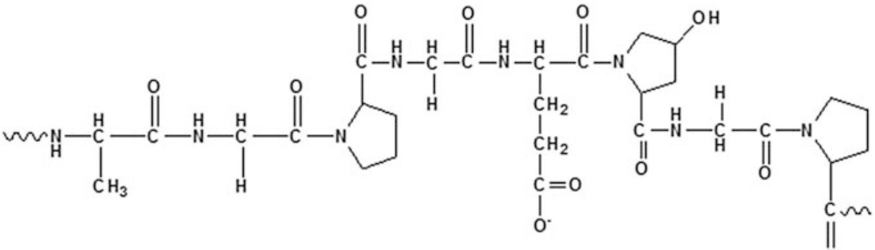

Gelatin

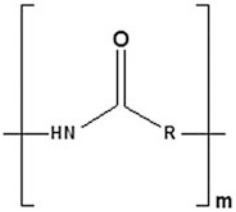

Zein

Fig. 2 Chemical structures of different polypeptide based biopolymers

CHNS analysis of carbon materials derived from collagen waste at elevated temperature abundantly showed the presence of carbon, oxygen and nitrogen in the range of 72–82, 6.2–15.4 and 2.9–13.6%, respectively [126]. The amount of zein adsorbed on the surface of montmorillonite (MMT) was determined by CHNS analysis; and it was found that biohybrids based on extracted phase (EXT) showed a lower amount of adsorbed protein than those prepared from precipitate [127].

3.2.2 FT-IR

Collagen is the principal structural constituent present in tissues; found most abundantly in the body. FT-IR spectra of type 1 collagen obtained from bone and skin tissues showed peaks of amide I at 1690, 1660, 1630 cm^{-1} corresponding to stretching vibration of C=O and amide III peak at 1235 cm^{-1} corresponding to stretching vibration of C–N and bending of N–H. Carbohydrate moieties present in collagen exhibited stretching vibration of C–O and C–O–C at 1100–1005 cm^{-1} [128, 129]. In another literature report, it was observed that the collagen-immobilized poly (3-hydroxybutyrate-co-3-hydroxyvalerate) (PHBV) and hydroxyapatite nanocomposite scaffolds showed IR peak at ~ 1722 cm^{-1} corresponding to vibrational bands of C=O present in PHBV whereas a peak at ~ 1039 cm^{-1} suggested the presence of PO_4^{3-} group exists in hydroxyapatite. In the same, characteristic peaks were observed at ~ 1640 and 1572 cm^{-1} for both amide I and amide II bonds of collagen, respectively [130]. The hybrid polymer/inorganic NCs of hyaluronan can be prepared either by in situ or ex situ method using both chemical and physical methods. The FTIR spectrum of HA/ZnO nanocomposite showed the peaks at ~ 3412, ~ 1616, ~ 1411, ~ 1149, ~ 1066, ~ 946, and ~ 661 cm^{-1}; thus confirming the presence of HA in the nanocomposite. The formation of ZnO nanoparticles was confirmed by distinct peak obtained at 441 cm^{-1}. The asymmetric sulfate stretching vibration band was observed at 1270 cm^{-1} and the peak at 1066 cm^{-1} was attributed to symmetric C–O vibration related to C–O–SO_3 or due to the weak C–OH stretching resulting from ZnO coordination. On the other hand, the peaks at ~ 1632 and 1433 cm^{-1} corresponded to stretching of (NH) C=O and $-COO^-$ or –OH groups, respectively. These peaks became strong and shifted slightly in the presence of ZnO nanoparticles, indicating that interactions between the (NH)C=O, –COOH, and OH groups of HA and ZnO nanoparticles [47]. Major peaks in FT-IR spectra of gelatin isolated from scales and bones of fish were observed in amide region. Scales gelatin showed amide-I and amide-III peaks along with phosphate stretching peaks which indicated the presence of calcium salts in scales gelatin sample. Interestingly, bone gelatin samples showed N–H stretching vibration of amide A at ~ 3340 cm^{-1} along with the amide-I, amide-II, and amide-III peaks [131]. FT-IR of glutaraldehyde-crosslinked gelatin nanoparticles showed a peak at 2927 cm^{-1} for asymmetric stretching of $-CH_2$ groups present in gelatin [132]. The FT-IR spectra of casein-acrylate TiO_2 nanocomposite suggested the successful grafting of acrylate monomers on the casein matrix.

Similar spectroscopic studies were also performed for hollow casein nanospheres [46] or poly(n-butyl acrylate)–casein NCs [133, 134]. Zein-based biodegradable nanopesticide containing geraniol and citronellal as active ingredients were synthesized and characterized using FT-IR. The spectra of zein showed bands between 3100 and 2800 cm^{-1}, which corresponds to –C–H groups present in fatty acids and amino acids. The spectrum of the geraniol loaded zein nanoparticles showed characteristic zein amides I and II peaks along with minimal shifts which may have resulted from the interactions of zein nanoparticles with the corresponding essential oil [135]. Similar FT-IR studies were also performed for soy protein isolate-carbon nanotube (SPI/CNTs) composites [136].

3.2.3 Powder XRD

XRD patterns for silica nanoparticles doped in hydroxyapatite/collagen and hydroxyapatite/gelatin showed crystalline planes for hydroxyapatite which was independent of doping material. Further, the crystallite size of hydroxyapatite gelatin silica nanocomposite and hydroxyapatite collagen silica composite was found to be 10.73 and 4.19 nm respectively [137]. In the X-ray diffraction pattern of HA/ZnO nanocomposite, prominent peaks were observed and assigned to the hexagonal wurtzite structure of nanometer ZnO particles with a degree of crystallinity [47]. The main peak in the XRD diffractogram of zein films with and without oleic acid appeared at the 2θ value of 19° which was susceptible to the number of cellulose nanofibrils (NF) present in the composite [138]. XRD patterns of raw zein and zein nanoparticles suggested amorphous nature for both the material which was further reduced in presence of high flow rate of CO_2 [139]. XRD pattern of gelatin and its corresponding drug loaded counterpart was found to show peaks at $2\theta = 20$ and 22° respectively, suggesting increase in the crystalline nature upon drug entrapment [132]. The XRD pattern for casein calcium phosphate nanocomposite revealed amorphous nature for the material [140].

3.2.4 NMR

Conformational study of a collagen peptide by ^{1}H NMR spectroscopy revealed an interesting temperature dependant 1:1:1 pattern of sharp resonance bands and slightly broader peak at $\sim$6.95 ppm, which was found to become even more broader with decreased temperature conditions. Further, ^{14}N–^{1}H spin-spin couplings were also observed because of quadrupolar relaxation which induces severe resonance broadening [141]. In another study, NMR spectra of collagen were investigated to compare between native and collagen present in biological tissues, such as bone, cartilage and skin. Characteristic signals from all collagen amino acids were obtained with a unique signal at 71.1 ppm, which can be assigned to the C_γ carbon of hydroxyproline. The ^{13}C MAS NMR spectra provided supports to resolve the fingerprint region of collagen whereas, ^{31}P cross polarization magic angle spinning

(CPMAS) studies on bone and bone implants have allowed to depict the biomineralization process [142]. ^{1}H-NMR spectra of methacrylic acid modified gelatin composite showed δ values between ~0.86 and 3.57 ppm which indicated characteristic peaks of methyl groups present in the amino acid residue of gelatin [143].

3.2.5 DLS and Zeta Potential

The particle size of zein nanoparticles was found to be ~300 nm which showed a constant decrease with increase in homogenization speed [144]. The zeta potential of zein nanoparticles coupled with gum arabic (GA) was found to be negative because of the presence of carboxylate groups in GA [145]. The DLS measurements revealed that the casein NCs showed the diameter of ~40–65 nm at pH 7.0 and the net charge was found to be negative [46].

3.2.6 UV-Vis and Fluorescence Studies

The presence of characteristic ZnO absorption band at 344 nm confirmed incorporation of ZnO into HA [47]. It was found that with increasing zein concentration, the plasmon resonance band of silver nanoparticles shifted from 458 to 428 nm and confirmed the formation of small size zein-silver nanoparticles [146]. The fluorescence of electrospun zein nanofibers conjugated with CdS QD (Quantum dot) showed emission at 561 nm. The emission intensity was found to be directly proportional to the CdS QD concentration. Further, the uniform fluorescence emission profile confirmed that the nanohybrid structure was stable in nature [147].

3.2.7 Circular Dichroism (CD) Spectroscopy

CD studies were carried out to confirm the presence of triple helix structure for type I collagen obtained from bovine calf skin [148]. Again, collagen obtained from streptococcal proteins showed unfolding of helix structure at 220 nm after denaturation [149]. CD spectroscopy studies were also carried out for gelatin composites [150].

3.2.8 TGA

The thermal stability of collagen was tested using TGA and results indicated that beyond denaturation temperature (T_d) collagen mostly converts into lower molecular weights elements. The specific viscosities started decreasing between 25 and 30 °C for skin collagen and between 30 and 35 °C for bone and muscle collagens [151]. TGA analysis showed that the in situ prepared silver/hyaluronan bionanocomposite increased the thermal and mechanical stability of resultant fibres [152].

Again, the TGA profile for the synthesized soy carbon nanotubes showed a weight loss of about 2% when the temperature was varied from 25 to 450 °C [136].

3.2.9 DSC

Collagen extracted from bovine tendon showed higher denaturation temperature for crosslinked collagen scaffolds due to highly stable triple helix conformation [153]. Collagen helix and their crosslinking nanocomposite showed changes in enthalpy and also in melting temperature [154]. Similar studies were also performed for casein and its developed composites [134].

3.2.10 SEM

SEM characterization of type I collagen extracted from equine tendon has been carried out to observe microscopic changes on the polymer surface [155]. Collagen obtained from bovine tendon suggested the presence of 50–150 μm pores on the nanocomposite surface [153]. FESEM image of HA/ZnO nanocomposite showed that ZnO nanoparticles of 3–8 nm size were present on the HA surface [47]. The majority of zein particles obtained via liquid-liquid dispersion was spherical in shape and possess particles size of less than 200 nm [144]. SEM images of prepared functionalized carbon nanotubes (FCNTs) showed homogeneous dispersion in the modified SPI adhesive, although individual CNTs could be observed as agglomerates [136]. Similar SEM studies were also carried out for SPI–MMT (montmorillonite) bio-nanocomposite [156] and casein NCs [46].

3.2.11 TEM

TEM studies were successfully carried out for HA-ZnO composites which showed the presence of 10–12 nm ZnO particles on the HA surface [47]. Similarly, gelatin nanoparticles of ~100 nm size were also observed [132]. Both zein and its corresponding silver-zein nanocomposite were characterized using TEM and size of the nanoparticles were found to be ~60 nm [146]. Similar studies were also carried out for casein and casein/calcium phosphate NCs [134, 140].

3.2.12 AFM

The AFM studies of collagen isolated from bovine vertebrae showed fibrils having a diameter in the range of 50–200 nm [157]. In another AFM study, the surface morphology of type 1 collagen showed thin film formation on nanocomposite surface [158]. Similar AFM studies were also performed for Zein–GA composites which suggested the formation of uniform spherical particles with average size of

143 nm and height of 43.8 nm [145]. AFM images revealed that casein nanospheres were spherical in shape with an average height of 21.0 ± 1.3 nm [134]. Further data on roughness factor for different casein NCs indicated that higher casein concentration allows homogeneous and smooth film formation [133]. The microstructure of the nanocomposite prepared from CNCs and soyabean oil was also characterized via AFM [159].

3.3 Synthetic Based Polymers

Eco-friendly synthetic based polymers have gained a lot of attention in current scenario due to their versatile nature and various applications in different fields. Different types of green NCs have been derived from modified synthetic polymers such as polylactic acid, poly(D,L-lactide-co-glycolide) (PLA, PLGA) and polyesters. This section draws the attention towards various techniques available for characterization of above mentioned synthetic biodegradable polymers (Fig. 3).

3.3.1 FT-IR

The FT-IR spectrum of PLGA-superparamagnetic iron oxide (SPIONs) nanocomposite with and without BSA showed prominent peak at ~2950–2850 cm^{-1}, assigned to C–H stretching of oleic acid on the SPIONs' surface whereas carboxylic acid present in PLGA showed sharp peaks at 1765–1750 cm^{-1} (C=O stretching), 1300–1090 cm^{-1} (C–C–O stretching), 1190–1085 cm^{-1} (C–O–C stretching) and 3100–2950 cm^{-1} (O–H stretching). However, BSA protein exhibited small signalling peaks at ~1650 cm^{-1} (C–O stretching of amide) and ~1540 cm^{-1} (N–H bending of amide) due to its lower concentration in the corresponding nanocomposite [160]. In another study, FT-IR spectra of PLA NCs showed peaks at ~2992, ~1373, and ~1454 cm^{-1} for stretching vibration, symmetric and asymmetric bending vibration of $-CH_3$ groups respectively. The nanocomposite of PLA poly (butylene adipate-co-terephthalate) nano-attapulgite (PLA/PBAT/AT) exhibited native PLA peak for stretching vibration of C=O group confirming the presence of

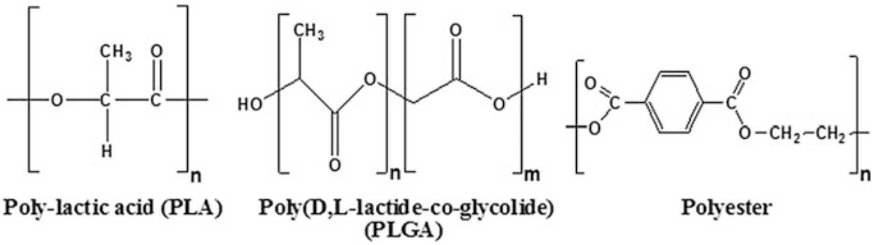

Fig. 3 Chemical structures of different synthetic biopolymers

PLA in the composite. Moreover, peaks at ~ 3057 and 740 cm^{-1} were attributed for stretching and bending vibrations of C–H present in benzene [25]. FT-IR spectra were observed for unsaturated polyester/styrene (UP) nanocomposite filled with nanodiamonds (NDs) containing carboxyl and methacrylate functional groups and exhibited a peak at 980 cm^{-1} which was assigned to the C–H out-of-plane bending in polyester molecules. Whereas, peak at 1730 cm^{-1} corresponds to C=O group which remained unchanged in UP/NDs nanocomposite [57].

3.3.2 Powder XRD

XRD pattern of pristine montmorillonite (Mt) and insulin-Mt-PLGA NCs showed a characteristic peak at a 2θ value of 6.4° (001) with a corresponding d spacing of 13.6 Å. However, no XRD pattern was observed for Mt due to its low concentration. Besides this, a hump corresponding to amorphous PLGA matrix also appeared at a 2θ value between 10 and 25°. XRD data depicted that Mt concentration could not influence the encapsulation efficiency of insulin in the composite [91]. XRD pattern observed for PLA and polylactic acid/poly-caprolactone (PLA/PCL) nanocomposite revealed their crystallinity indices to be 31.43, and 17.34% respectively. Further, two peaks of PLA at a 2θ value of ~ 16.4° and ~ 22.6° were observed from the same studies [161].

3.3.3 NMR

^{13}C solid-state NMR spectra of chitosan-PLA modified CNT NCs showed peaks at 65 and between 20 and 22 ppm for chitosan-CNTs and the composite respectively [162]. In another literature report, ^{1}H NMR spectra suggested chemical shift in poly (D,L-lactide-co-glycolide) (PLGA) copolymer with δ value between 1.46–1.68, 4.67–4.90 and 5.13–5.30 ppm assigned to –CH_3, –CH_2, and –CH functional groups respectively [56]. ^{1}H NMR of unsaturated polyester-styrene cured resin showed the integration of the broad bands at ~ 6.8 and 0.8–4.0 ppm which were assigned to the ring protons of styrene and esterified fumarate residues of aliphatic chain [163].

3.3.4 TGA

It was found that carbon dot (CD) conjugation improved the thermostability of polyesters by shifting the initial degradation temperature of the nanocomposite towards higher temperature. The increased thermostability of the NCs can be ascribed to high cross-linking density and secondary interactions imparted by CD with the polyester chains [164].

3.3.5 DSC

The positive influence of CNTs on the thermo-mechanical properties of unsaturated polyester NCs (UP) was studied using DSC. DSC thermogram provided the information of chain intercalation and thermal transition for the studied NCs. Interestingly, the NCs exhibited a split in the melting endotherm whereas the corresponding polyester showed a single peak, suggesting bond formation between CNT and UP for the former case [57].

3.3.6 SEM

SEM analysis of the nanocomposite prepared using iron oxide and lysine/BSA modified PLGA were studied and was used for protein antigen delivery and immune stimulation in dendritic cells [160]. The surface morphology of the fractured PLA nanocomposite (PLA/PBAT/AT) was observed by SEM studies [25]. In a separate study, the native PLA showed irregular microfibril structure compared to PLA nanocomposite (PLA/PCL) when both were dissolved in the phosphate saline buffer [161].

3.3.7 TEM

The TEM studies suggested that the mean particle size of Fe_3O_4 and Fe_3O_4-3-(trimethoxysilyl)-propyl methacrylate (MPTMS) was 8.8 ± 1.8 and 8.7 ± 1.8 nm respectively. Further, TEM images of Fe_3O_4-MPTMS-PLGA NCs showed 1–2 nm polymer coating thickness [165]. The surface morphology of PLA and PLA nanocomposite (PLA/PBAT/AT) were also studied using TEM [25].

The signature peaks for the described eco-friendly polymers have been summarized in Scheme 2.

4 Future Perspectives

For the sustainable development of the society, next-generation eco-friendly polymer composites are required to produce from renewable sources which possess superior physicochemical and biological properties. Globally BASF, Nature Works, Arkema, Novamont, and Plantic has been found to be the major player which governs the mass production of different polymers like- polylactic acid, starch-based polymer etc. contributing in several industries like—food, healthcare, and agriculture. Moreover, it is expected that this area will witness an increase in the CAGR by a significant amount at the end of 2021. Thus industries are changing their focus toward exploring the possibilities of biodegradable polymers. NCs offer

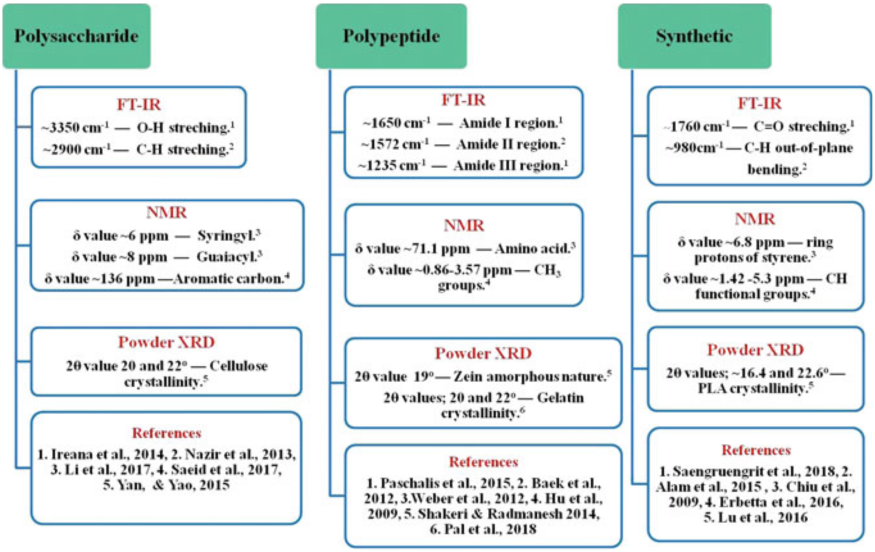

Scheme 2 Illustrative representation of the characteristic FT-IR, NMR and powder XRD peaks observed for different eco-friendly polymers

some great advantages over microcomposites because these possess improved strength and hardness. For the best utilization of the isolated eco-friendly polymers and their corresponding composites, proper characterization needs to be done.

Acknowledgements The authors would like to thank Director, CSIR-IHBT for his constant support and encouragement. AA acknowledges financial assistance in the form of project grant MLP-0201 from CSIR and GAP-0214 (EMR/2016/003027) from DST, Government of India. AKS, CS, SMSA acknowledge Academy of Scientific and Innovative Research (AcSIR) and CSIR-GATE and DBT for their respective JRF fellowship. AKS, CS and SMSA have contributed equally to this book chapter. The CSIR-IHBT communication number of this manuscript is 4254.

References

1. Camargo PHC, Satyanarayana KG, Wypych F (2009) Nanocomposites: synthesis, structure, properties and new application opportunities. Mater Res 12(1):1–39
2. Davidson S (2008) Sustainable bioenergy: genomics and biofuels development. Nat Edu 1(1):175–181
3. Iwata T (2015) Biodegradable and bio-based polymers: future prospects of eco-friendly plastics. Angew Chem Int Ed 54(11):3210–3215
4. Ray SS, Bousmina M (2005) Biodegradable polymers and their layered silicate nanocomposites: in greening the 21st century materials world. Prog Mater Sci 50(8):962–1079
5. Joshi G, Naithani S, Varshney VK, Bisht SS, Rana V, Gupta PK (2015) Synthesis and characterization of carboxymethyl cellulose from office waste paper: a greener approach towards waste management. Waste Manag 38:33–40

6. Singhsa P, Narain R, Manuspiya H (2018) Physical structure variations of bacterial cellulose produced by different Komagataeibacter xylinus strains and carbon sources in static and agitated conditions. Cellulose 25(3):1571–1581
7. Tuli M, Gurumayum S, Kaur S, Nagal S, Attri I (2015) Isolation and screening of cellulolytic fungi by baiting method from soils of Jalandhar. Res J Pharm Biol Chem Sci 6(2):375–380
8. Singla R, Soni S, Kulurkar PM, Kumari A, Mahesh S, Patial V, Yadav SK (2017) In situ functionalized nanobiocomposites dressings of bamboo cellulose nanocrystals and silver nanoparticles for accelerated wound healing. Carbohydr Polym 155:152–162
9. Phanthong P, Reubroycharoen P, Hao X, Xu G, Abudula A, Guan G (2018) Nanocellulose: extraction and application. CRC 1(1):32–43
10. Fatah IYA, Khalil HPS, Hossain MS, Aziz AA, Davoudpour Y, Dungani R, Bhat A (2014) Exploration of a chemo-mechanical technique for the isolation of nanofibrillated cellulosic fiber from oil palm empty fruit bunch as a reinforcing agent in composites materials. Polymers 6(10):2611–2624
11. Shao C, Wang M, Chang H, Xu F, Yang J (2017) A self-healing cellulose nanocrystal-poly (ethylene glycol) nanocomposite hydrogel via diels-alder click reaction. ACS Sustain Chem Eng 5(7):6167–6174
12. Li J, Wei X, Wang Q, Chen J, Chang G, Kong L, Liu Y (2012) Homogeneous isolation of nanocellulose from sugarcane bagasse by high pressure homogenization. Carbohydr Polym 90(4):1609–1613
13. Wang W, Mozuch MD, Sabo RC, Kersten P, Zhu JY, Jin Y (2015) Production of cellulose nanofibrils from bleached eucalyptus fibers by hyperthermostable endoglucanase treatment and subsequent microfluidization. Cellulose 22(1):351–361
14. Alemdar A, Sain M (2008) Isolation and characterization of nanofibers from agricultural residues—wheat straw and soy hulls. Bioresour Technol 99(6):1664–1671
15. Chen L, Wang Q, Hirth K, Baez C, Agarwal UP, Zhu JY (2015) Tailoring the yield and characteristics of wood cellulose nanocrystals (CNC) using concentrated acid hydrolysis. Cellulose 22(3):1753–1762
16. Lindblad Soderqvist M, Albertsson AC, Ranucci E, Laus M, Giani E (2005) Biodegradable polymers from renewable sources: rheological characterization of hemicellulose-based hydrogels. Biomacromolecules 6(2):684–690
17. Muchlisyam JS, Harahap U (2016) Hemicellulose: Isolation and its application in pharmacy. Handbook of sustainable polymers: Processing and applications, p 305–339
18. Dereca W, Nuruddin Md, Mahesh H, Alfred T-N, Shaik J (2015) Extraction and characterization of lignin from different biomass resources. JMRT 4(1):26–32
19. Hu L, Pan H, Zhou Y, Zhang M (2011) Methods to improve lignin's reactivity as a phenol substitute and as a replacement for other phenolic compounds: a brief review. BioResources 6(3):3515–3525
20. Kuhad R, Singh A (2007) Lignocellulose biotechnology: future prospects. I.K. International Publishing House, Delhi
21. Harmsen PFH, Huijgen WJJ, Bermúdez López LM, Bakker RRC (2010) Literature review of physical and chemical pretreatment processes for lignocellulosic biomass. Energy Research Centre of the Netherlands (ECN), ECN-E–10-013
22. Lee SH, Doherty TV, Linhardt RJ, Dordick JS (2009) Ionic liquid-mediated selective extraction of lignin from wood leading to enhanced enzymatic cellulose hydrolysis. Biotechnol Bioeng 102(5):1368–1376
23. Velez J, Thies MC (2016) Liquid lignin from the SLRP process: the effect of process conditions and black liquor properties. J Wood Chem Technol 36:27–41
24. Shi H, Fatehi P, Xiao H, Ni Y (2012) A process for isolating lignin of pre-hydrolysis liquor of Kraft pulping process based on surfactant and calcium oxide treatments. Biochem Eng J68:19–24

25. Zhou L, Santomauro F, Fan J, Macquarrie D, Clark J, Chuck CJ, Budarin V (2017) Fast microwave-assisted acidolysis: a new biorefinery approach for the zero-waste utilisation of lignocellulosic biomass to produce high quality lignin and fermentable saccharides. Faraday Discuss 202:351–370
26. Bychkov AL, Podgorbunskikh EM, Ryabchikova EI, Lomovsky OI (2018) The role of mechanical action in the process of the thermomechanical isolation of lignin. Cellulose 25:1–5
27. Reddy DK, Bhotmange MG (2013) Isolation of starch from rice (*Oryza sativa L.*) and its morphological study using scanning electron microscopy. IJAFST 4(9): 859–866
28. El-Sheikh Manal A (2017) New technique in starch nanoparticles synthesis. Carbohydr Polym 176:214–219
29. Chen Y, Liu C, Chang PR, Anderson DP, Huneault MA (2009) Pea starch-based composite films with pea hull fibers and pea hull fiber-derived nanowhiskers. Polym Eng Sci 49(2): 369–378
30. Zheng H, Ai F, Chang PR, Huang J, Dufresne A (2009) Structure and properties of starch nanocrystal-reinforced soy protein plastics. Polym Composite 30(4):474–480
31. Kim J-Y, Park D-J, Lim S-T (2008) Fragmentation of waxy rice starch granules by enzymatic hydrolysis. Cereal Chem 85(2):182–187
32. Liu D, Wu Q, Chen H, Chang RR (2009) Transitional properties of starch colloid with particle size reduction from micro to nanometer. J Colloid Interface Sci 339(1):117–124
33. LeCorre D, Vahanian E, Dufresne A, Bras J (2012) Enzymatic pretreatment for preparing starch nanocrystals. Biomacromolecules 13(1):132–137
34. Espinosa Solis V, Jane J, Bello Perez LA (2009) Physicochemical characteristics of starches from unripe fruits of mango and banana. Starke 61(5):291–299
35. Haque S, Md S, Sahni JK, Ali J, Baboota S (2014) Development and evaluation of brain targeted intranasal alginate nanoparticles for treatment of depression. J Psychiatr Res 48(1): 1–12
36. Xu X, Qu T, Fan L, Chen X, Gao M, Zhang J, Guo T (2016) Preparation of pH-and magnetism-responsive sodium alginate/Fe_3O_4@ HNTs nanocomposite beads for controlled release of granulysin. RSC Adv 6(113):111747–111753
37. Anderson TJ, Lamsal BP (2011) Zein extraction from corn, corn products, and coproducts and modifications for various applications: a review. Cereal Chem 88(2):159–173
38. Dickey LC, Parris N, Craig JC, Kurantz MJ (2001) Ethanolic extraction of zein from maize. Ind Crops Prod 13(1):67–76
39. Preece KE, Hooshyar N, Zuidam NJ (2017) Whole soybean protein extraction processes: a review. Innovative Food Sci Emerg Technol 43:163–172
40. Schmidt MM, Dornelles RCP, Mello RO, Kubota EH, Mazutti MA, Kempka AP, Demiate IM (2016) Collagen extraction process. Int Food Res J 23(3):913–922
41. Shyni K, Hema GS, Ninan G, Mathew S, Joshy CG, Lakshmanan PT (2014) Isolation and characterization of gelatin from the skins of skipjack tuna (*Katsuwonus pelamis*), dog shark (*Scoliodon sorrakowah*), and rohu (*Labeo rohita*). Food Hydrocoll 39:68–76
42. Anchana D, Kamatchi P, Leela K (2016) Extraction, characterization and application of gelatin from *Carcharhinus amblyrhyncho* and *Sphyraena barracuda*. IOSR-JBB 2(6):40–49
43. Du L, Keplová L, Khiari Z, Betti M (2014) Preparation and characterization of gelatin from collagen biomass obtained through a pH-shifting process of mechanically separated turkey meat. Poult Sci 93(4):989–1000
44. Fernando LAT, Poblete MRS, Ongkiko AGM, Diaz LJL (2016) Chitin extraction and synthesis of chitin-based polymer films from Philippine Blue Swimming Crab (*Portunus pelagicus*) shells. Procedia Chem 19:462–468
45. Kumari S, Rath PK (2014) Extraction and characterization of chitin and chitosan from (*Labeo rohit*) fish scales. Procedia Materials Science 6:482–489
46. Xiao-Zhou S, Hong-Ru W, Mian H (2014) Characterization of the casein/keratin self-assembly nanomicelles. J Nanomater 2014(183815):1–7

47. Namvar F, Azizi S, Rahman HS, Mohamad R, Rasedee A, Soltani M, Rahim RA (2016) Green synthesis, characterization, and anticancer activity of hyaluronan/zinc oxide nanocomposite. OncoTargets Ther 9:4549
48. Amagai I, Tashiro Y, Ogawa H (2009) Improvement of the extraction procedure for hyaluronan from fish eyeball and the molecular characterization. Fish Sci 75(3):805–810
49. Guhados G, Wan W, Hutter JL (2005) Measurement of the elastic modulus of single bacterial cellulose fibers using atomic force microscopy. Langmuir 21(14):6642–6646
50. Huang HC, Chen LC, Lin SB, Hsu CP, Chen HH (2010) In situ modification of bacterial cellulose network structure by adding interfering substances during fermentation. Bioresour Technol 101(15):6084–6091
51. Zeng X, Small DP, Wan W (2011) Statistical optimization of culture conditions for bacterial cellulose production by *Acetobacter xylinum* BPR 2001 from maple syrup. Carbohydr Polym 85(3):506–513
52. Sheoran SK, Dubey KK, Tiwari DP, Singh BP (2012) Directive production of pullulan by altering cheap source of carbons and nitrogen at 5l bioreactor level. ISRN Chemical Engineering 2012:1–5
53. Shehata AN, Darwish DA, Masoud HM (2016) Extraction, purification and characterization of endo-acting pullulanase Type I from white edible mushrooms. J Appl Pharm Sci 6(01): 147–152
54. Jamshidian M, Tehrany EA, Imran M, Jacquot M, Desobry S (2010) Poly-lactic acid: production, applications, nanocomposites, and release studies. Compr Rev Food Sci Food Saf 9(5):552–571
55. Danhier F, Ansorena E, Silva JM, Coco R, Le Breton A, Preat V (2012) PLGA-based nanoparticles: an overview of biomedical applications. J Control Release 161(2):505–522
56. Erbetta CDAC, Alves RJ, Resende JM, de Souza Freitas RF, de Sousa RG (2012) Synthesis and characterization of poly(D, L-lactide-co-glycolide) copolymer. J Biomater Nanobiotechnol 3(02):208
57. Beg MDH, Alam AM, Yunus RM, Mina MF (2015) Improvement of interaction between pre-dispersed multi-walled carbon nanotubes and unsaturated polyester resin. J Nanopart Res 17(1):53
58. Saeid N, Omid Z, Yousef Mojtaba, Saba A, Minoo N (2017) Catalyzed synthesis characterization of a novel lignin-based curing agent for the curing of high-performance epoxy resin. Polymers 9(7):266
59. Le DM, Nielsen AD, Sørensen HR, Meyer AS (2017) Characterisation of authentic lignin biorefinery samples by Fourier transform infrared spectroscopy and determination of the chemical formula for lignin. BioEnerg Res 10(4):1025–1035
60. Abraham E, Kam D, Nevo Y, Slattegard R, Rivkin A, Lapidot S, Shoseyov O (2016) Highly modified cellulose nanocrystals and formation of epoxy-nanocrystalline cellulose (CNC) nanocomposites. ACS Appl Mater Interfaces 8(41):28086–28095
61. Luduena LN, Vecchio A, Stefani PM, Alvarez VA (2013) Extraction of cellulose nanowhiskers from natural fibers and agricultural byproducts. Fibers Polym 14(7):1118–1127
62. Haafiz MM, Eichhorn SJ, Hassan A, Jawaid M (2013) Isolation and characterization of microcrystalline cellulose from oil palm biomass residue. Carbohydr Polym 93(2):628–634
63. Spiridonov VV, Panova IG, Afanasov MI, Zezin SB, Sybachin AV, Yaroslavov AA (2018) Water-Soluble magnetic nanocomposites based on carboxymethyl cellulose and iron (III) oxide. Polym Sci Ser B 60(1):116–121
64. Cardoso GV, Mello LRDS, Zanatta P, Cava S, Raubach CW, Moreira ML (2018) Physico-chemical description of titanium dioxide–cellulose nanocomposite formation by microwave radiation with high thermal stability. Cellulose 25(4):2331–2341
65. Ayoub A, Venditti RA, Pawlak JJ, Salam A, Hubbe MA (2013) Novel hemicellulose–chitosan biosorbent for water desalination and heavy metal removal. ACS Sustain Chem Eng 1(9):1102–1109

66. Badshah M, Ullah H, Khan AR, Khan S, Park JK, Khan T (2018) Surface modification and evaluation of bacterial cellulose for drug delivery. Int J Biol Macromol 113:526–533
67. Foong CY, Hamzah MSA, Razak SIA, Saidin S, Nayan NHM (2018) Influence of poly (lactic acid) layer on the physical and antibacterial properties of dry bacterial cellulose sheet for potential acute wound healing materials. Fibers Polym 19(2):263–271
68. Vijayalakshmi K, Gomathi T, Sudha PN (2014) Preparation and characterization of nanochitosan/sodium alginate/microcrystalline cellulose beads. Der Pharmacia Lettre 6(4): 65–77
69. Krishnaveni B, Ragunathan R (2015) Extraction and Characterization of chitin and chitosan from *F. solani* CBNR BKRR, synthesis of their bionanocomposites and study of their productive application. J Pharm Sci Res 7(4):197–205
70. Shanthi P, Kothai S (2015) Synthesis and characterization of chitosan with incorporated herb —a novel bionano composite. Int J Chemtech Res 8(8):208–214
71. Silva NH, Vilela C, Almeida A, Marrucho IM, Freire CS (2018) Pullulan-based nanocomposite films for functional food packaging: exploiting lysozyme nanofibers as antibacterial and antioxidant reinforcing additives. Food Hydrocoll 77:921–930
72. Mitić Ž, Cakić M, Nikolić GM, Nikolić R, Nikolić GS, Pavlović R, Santaniello E (2011) Synthesis, physicochemical and spectroscopic characterization of copper (II)-polysaccharide pullulan complexes by UV–vis, ATR-FTIR, and EPR. Carbohydr Res 346(3):434–441
73. Xu F, Yu J, Tesso T, Dowell F, Wang D (2013) Qualitative and quantitative analysis of lignocellulosic biomass using infrared techniques: a mini-review. Appl Energy 104:801–809
74. Sills DL, Gossett JM (2012) Using FTIR to predict saccharification from enzymatic hydrolysis of alkali-pretreated biomasses. Biotechnol Bioeng 109(2):353–362
75. Tian X, Rehmann L, Xu CC, Fang Z (2016) Pretreatment of eastern white pine (*Pinus strobes* L.) for enzymatic hydrolysis and ethanol production by organic electrolyte solutions. ACS Sustain Chem Eng 4(5):2822–2829
76. Kubo S, Kadla JF (2005) Hydrogen bonding in lignin: a Fourier transform infrared model compound study. Biomacromolecules 6(5):2815–2821
77. Ma X, Jian R, Chang PR, Yu J (2008) Fabrication and characterization of citric acid-modified starch nanoparticles/plasticized-starch composites. Biomacromolecules 9(11): 3314–3320
78. Poletto M, Pistor V, Zattera AJ (2013) Structural characteristics and thermal properties of native cellulose. In: Cellulose-fundamental aspects. InTech, p 45–68
79. El Oudiani A, Chaabouni Y, Msahli S, Sakli F (2011) Crystal transition from cellulose I to cellulose II in NaOH treated *Agave americana* L. fibre. Carbohydr Polym 86(3):1221–1229
80. Huang HD, Liu CY, Zhou D, Jiang X, Zhong GJ, Yan DX, Li ZM (2015) Cellulose composite aerogel for highly efficient electromagnetic interference shielding. J Mater Chem A 3(9):4983–4991
81. Dietrich K, Hernandez-Mejia C, Verschuren P, Rothenberg G, Shiju NR (2017) One-pot selective conversion of hemicellulose to xylitol. Org Process Res Dev 21(2):165–170
82. Peng XW, Ren JL, Zhong LX, Sun RC (2011) Nanocomposite films based on xylan-rich hemicelluloses and cellulose nanofibers with enhanced mechanical properties. Biomacromolecules 12(9):3321–3329
83. Zhong C, Zhang GC, Liu M, Zheng XT, Han PP, Jia SR (2013) Metabolic flux analysis of *Gluconacetobacter xylinus* for bacterial cellulose production. Appl Microbiol Biotechnol 97 (14):6189–6199
84. Ramírez JAÁ, Hoyos CG, Arroyo S, Cerrutti P, Foresti ML (2016) Acetylation of bacterial cellulose catalyzed by citric acid: use of reaction conditions for tailoring the esterification extent. Carbohydr Polym 153:686–695
85. Chen K, Ling Y, Cao C, Li X, Chen X, Wang X (2016) Chitosan derivatives/reduced graphene oxide/alginate beads for small-molecule drug delivery. Mater Sci Eng C 69:1222–1228

86. Ramesan MT, Siji C, Kalaprasad G, Bahuleyan BK, Al-Maghrabi MA (2018) Effect of silver doped zinc oxide as nanofiller for the development of biopolymer nanocomposites from chitin and cashew gum. J Polym Environ 26(7):2983–2991
87. Köhnke J, Fürst C, Unterweger C, Rennhofer H, Lichtenegger HC, Keckes J, Emsenhuber G, Liebner F, Gindl-Altmutter W (2016) Carbon microparticles from organosolv lignin as filler for conducting poly(lactic acid). Polymers 8(6):205
88. Shivananda CS, Rao BL, Madhukumar R, Sarojini BK, Somashekhar R, Asha, S, Sangappa Y (2016) Silk fibroin/pullulan blend films: preparation and characterization. In: AIP conference proceedings, vol 1731(1). AIP Publishing, p 070013
89. Trovatti E, Fernandes SC, Rubatat L, Freire CS, Silvestre AJ, Neto CP (2012) Sustainable nanocomposite films based on bacterial cellulose and pullulan. Cellulose 19(3):729–737
90. Tzhayik O, Pulidindi IN, Gedanken A (2014) Forming nanospherical cellulose containers. Ind Eng Chem Res 53(36):13871–13880
91. Lal S, Perwez A, Rizvi MA, Datta M (2017) Design and development of a biocompatible montmorillonite PLGA nanocomposites to evaluate in vitro oral delivery of insulin. Appl Clay Sci 147:69–79
92. Goundalkar MJ, Corbett DB, Bujanovic BM (2014) Comparative analysis of milled wood lignins (MWLs) isolated from sugar maple (SM) and hot water extracted sugar maple (ESM). Energies 7(3):1363–1375
93. Pu Y, Cao S, Ragauskas AJ (2011) Application of quantitative 31P NMR in biomass lignin and biofuel precursors characterization. Energy Environ Sci 4(9):3154–3166
94. Mascheroni E, Rampazzo R, Ortenzi MA, Piva G, Bonetti S, Piergiovanni L (2016) Comparison of cellulose nanocrystals obtained by sulfuric acid hydrolysis and ammonium persulfate, to be used as coating on flexible food-packaging materials. Cellulose 23(1): 779–793
95. Astruc J, Nagalakshmaiah M, Laroche G, Grandbois M, Elkoun S, Robert M (2017) Isolation of cellulose-II nanospheres from flax stems and their physical and morphological properties. Carbohydr Polym 178:352–359
96. Kishani S, Vilaplana F, Xu W, Xu C, Wagberg (2018) Solubility of softwood hemicelluloses. Biomacromolecules 19(4):1245–1255
97. Madhusudhan KN, Meghana PB, Vinaya Rani G, Moorthy SM, Mary-Josepha AV (2017) Extraction and characterization of chitin and chitosan from *Aspergillus niger*, synthesis of silver-chitosan nanocomposites and evaluation of their antimicrobial potential. Journal of Advances in Biotechnology 6(3):939–945
98. Mushi NE, Utsel S, Berglund LA (2014) Nanostructured biocomposite films of high toughness based on native chitin nanofibers and chitosan. Front Chem 2(99):1–11
99. Coseri S, Spatareanu A, Sacarescu L, Socoliuc V, Sorin Stratulat I, Harabagiu V (2016) Pullulan: a versatile coating agent for superparamagnetic iron oxide nanoparticles. J Appl Polym Sci 133(5):42926(1–9)
100. Li G, Sun Y, Liu H (2018) Gold-carboxymethyl cellulose nanocomposites greenly synthesized for fluorescent sensitive detection of Hg(II). J Cluster Sci 29(1):177–184
101. Li J, Zhang J, Zha S, Gao Q, Li J, Zhang Q (2017) Fast curing biobased phenolic resins via lignin demethylated under mild reaction condition. Polymers 9(9):428
102. Anandhavelu S, Thambidurai S (2012) Preparation of chitosan-ZnO nanocomposite from chitin polymer. Adv Mat Res 584:234–238
103. Putnam CD, Hamme M, Hura GL, Tainer JA (2007) X-ray solution scattering (SAXS) combined with crystallography and computation: defining accurate macromolecular structures, conformations and assemblies in solution. Q Rev Biophys 40(3):191–285
104. Yang H, Yan R, Chen H, Lee DH, Zheng C (2007) Characteristics of hemicellulose, cellulose and lignin pyrolysis. Fuel 86(12–13):1781–1788
105. Nagalakshmaiah M, Mortha G, Dufresne A (2016) Structural investigation of cellulose nanocrystals extracted from chili leftover and their reinforcement in cariflex-IR rubber latex. Carbohydr Polym 136:945–954

106. Zhao W, Odelius K, Edlund U, Zhao C, Albertsson AC (2015) In situ synthesis of magnetic field-responsive hemicellulose hydrogels for drug delivery. Biomacromolecules 16(8):2522–2528
107. Malagurski I, Levic S, Mitric M, Pavlovic V, Dimitrijevic-Brankovic S (2018) Bimetallic alginate nanocomposites: new antimicrobial biomaterials for biomedical application. Mater Lett 212:32–36
108. Praveen P, Rao V (2014) Synthesis and thermal studies of chitin/AgCl nanocomposite. Procedia Materials Science 5(2014):1155–1159
109. Deng J, Xiong T, Wang H, Zheng A, Wang Y (2016) Effects of cellulose, hemicellulose, and lignin on the structure and morphology of porous carbons. ACS Sustain Chem Eng 4(7): 3750–3756
110. Gokila S, Gomathi T, Sudha PN, Anil S (2017) Removal of the heavy metal ion chromiuim (VI) using chitosan and alginate nanocomposites. Int J Biol Macromol 104:1459–1468
111. Morin A, Dufresne A (2002) Nanocomposites of chitin whiskers from Riftia tubes and poly (caprolactone). Macromolecules 35(6):2190–2199
112. Alahmadi NS, Betts JW, Heinze T, Kelly SM, Koschella A, Wadhawan JD (2018) Synthesis and antimicrobial effects of highly dispersed, cellulose-stabilized silver/cellulose nanocomposites. RSC Adv 8(7):3646–3656
113. Mathew L, Joshy MK, Joseph R (2011) Isora fibre: a natural reinforcement for the development of high performance engineering materials. In: Cellulose fibers: bio-and nano-polymer composites. Springer, Berlin, Heidelberg, p 291–324
114. Uraki Y, Nemoto J, Otsuka H, Tamai Y, Sugiyama J, Kishimoto T, Shimomura M (2007) Honeycomb-like architecture produced by living bacteria, *Gluconacetobacter xylinus*. Carbohydr Polym 69(1):1–6
115. Motshekga SC, Ray SS, Maity A (2018) Synthesis and characterization of alginate beads encapsulated zinc oxide nanoparticles for bacteria disinfection in water. J Colloid Interface Sci 512:686–692
116. PM V, Thomas S (2011) Preparation and characterization of chitin nanowhiskers and their polymer nanocomposites. Int J Polym Technol 3(1):35–44
117. Krull SM, Ma Z, Li M, Davé RN, Bilgili E (2016) Preparation and characterization of fast dissolving pullulan films containing BCS class II drug nanoparticles for bioavailability enhancement. Drug Dev Ind Pharm 42(7):1073–1085
118. Selig MJ, Viamajala S, Decker SR, Tucker MP, Himmel ME, Vinzant TB (2007) Deposition of lignin droplets produced during dilute acid pretreatment of maize stems retards enzymatic hydrolysis of cellulose. Biotechnol Prog 23(6):1333–1339
119. Yan CF, Yu HY, Yao JM (2015) One-step extraction and functionalization of cellulose nanospheres from lyocell fibers with cellulose II crystal structure. Cellulose 22(6):3773–3788
120. Parambath Kanoth B, Claudino M, Johansson M, Berglund LA, Zhou Q (2015) Biocomposites from natural rubber: synergistic effects of functionalized cellulose nanocrystals as both reinforcing and cross-linking agents via free-radical thiol–ene chemistry. ACS Appl Mater Interfaces 7(30):16303–16310
121. Tian D, Hu J, Bao J, Chandra RP, Saddler JN, Canhui Lu (2017) Lignin valorization: lignin nanoparticles as high-value bio-additive for multifunctional nanocomposites. Biotechnol Biofuels 10(1):192
122. Geng L, Peng X, Zhan C, Naderi A, Sharma PR, Mao Y, Hsiao BS (2017) Structure characterization of cellulose nanofiber hydrogel as functions of concentration and ionic strength. Cellulose 24(12):5417–5429
123. Vilcinskas K, Zlopasa J, Jansen K, Mulder FM, Picken SJ, Koper GJ (2016) Water sorption and diffusion in (reduced) graphene oxide-alginate biopolymer nanocomposites. Macromol Mater Eng 301(9):1049–1063
124. Mathew AP, Laborie MPG, Oksman K (2009) Cross-linked chitosan/chitin crystal nanocomposites with improved permeation selectivity and pH stability. Biomacromolecules 10(6): 1627–1632

125. Kittle JD, Wang C, Qian C, Zhang Y, Zhang M, Roman M, Esker AR (2012) Ultrathin chitin films for nanocomposites and biosensors. Biomacromolecules 13(3):714–718
126. Ashokkumar M, Narayanan NT, Reddy ALM, Gupta BK, Chandrasekaran B, Talapatra S, Thanikaivelan P (2012) Transforming collagen wastes into doped nanocarbons for sustainable energy applications. Green Chem 14(6):1689–1695
127. Alcântara AC, Darder M, Aranda P, Ruiz-Hitzky E (2016) Effective intercalation of zein into Na-montmorillonite: role of the protein components and use of the developed biointerfaces. Beilstein J Nanotechnol 7:1772
128. Belbachir K, Noreen R, Gouspillou G, Petibois C (2009) Collagen types analysis and differentiation by FTIR spectroscopy. Anal Bioanal Chem 395(3):829–837
129. Paschalis EP, Gamsjaeger S, Tatakis DN, Hassler N, Robins SP, Klaushofer K (2015) Fourier transform infrared spectroscopic characterization of mineralizing type I collagen enzymatic trivalent cross-links. Calcif Tissue Int 96(1):18–29
130. Baek JY, Xing ZC, Kwak G, Yoon KB, Park SY, Park LS, Kang IK (2012) Fabrication and characterization of collagen-immobilized porous PHBV/HA nanocomposite scaffolds for bone tissue engineering. J Nanomater 2012:1–11
131. Zakaria S, Bakar NHA (2015) Extraction and characterization of gelatin from Black tilapia (Oreochromis niloticus) scales and bones. In: International conference on advances in science, engineering, technology & natural resources (ICASETNR-15), Kota Kinabalu (Malaysia), p 77–80
132. Pal A, Bajpai J, Bajpai AK (2018) Easy fabrication and characterization of gelatin nanocarriers and in vitro investigation of swelling controlled release dynamics of paclitaxel. Polym Bull 75(10):4691–4711
133. Picchio ML, Ronco LI, Passeggi MC, Minari RJ, Gugliotta LM (2017) Poly (n-butyl acrylate)–casein nanocomposites as promising candidates for packaging films. J Polym Environ 26(6):2579–2587
134. Zhang F, Ma J, Xu Q, Zhou J, Simion D, Carmen G, Li Y (2016) Correction to hollow casein-based polymeric nanospheres for opaque coatings. ACS Appl Mater Interfaces 8(24):15856–15856
135. Oliveira JL, Campos EVR, Pereira ADES, Pasquoto T, Lima R, Grillo R, Fraceto LF (2018) Zein nanoparticles as eco-friendly carrier systems for botanical repellents aiming sustainable agriculture. J Agric Food Chem 66(6):1330–1340
136. Sadare OO, Daramola MO, Afolabi AS (2015) Preparation and characterization of nanocomposite soy-carbon nanotubes (SPI/CNTs) adhesive from soy protein isolate. In: Proceedings of the world congress on engineering, vol 2. London, U.K., p 1–3
137. Najafizadeha F, Sadjadia MAS, Fatemib SJ, Mobarakehc MK, Afshard RM (2016) A comparison between biocompatibilities of nanocomposites of silica doped in HA/collagen and those doped in HA/gelatin. OJC 32(3):1551–1557
138. Shakeri A, Radmanesh S (2014) Preparation of cellulose nanofibrils by high-pressure homogenizer and Zein composite films. Adv Mat Res 829:534–538
139. Li S, Zhao Y (2017) Preparation of zein nanoparticles by using solution-enhanced dispersion with supercritical CO_2 and elucidation with computational fluid dynamics. Int J Nanomedicine 12:3485
140. Ding GJ, Zhu YJ, Cheng GF, Ruan YJ, Qi C, Lu BQ, Wu J (2016) Porous microspheres of casein/amorphous calcium phosphate nanocomposite: room temperature synthesis and application in drug delivery. Curr Nanosci 12(1):70–78
141. Consonni R, Santomo L, Tenni R, Longhi R, Zetta L (1998) Conformational study of a collagen peptide by 1H NMR spectroscopy: observation of the 14N–1H spin-spin coupling of the Arg guanidinium moiety in the triple-helix structure. FEBS Lett 436(2):243–246
142. Weber F, Böhme J, Scheidt HA, Gründer W, Rammelt S, Hacker M, Huster D (2012) 31P and 13C solid-state NMR spectroscopy to study collagen synthesis and biomineralization in polymer-based bone implants. NMR Biomed 25(3):464–475

143. Hu X, Ma L, Wang C, Gao C (2009) Gelatin hydrogel prepared by photo-initiated polymerization and loaded with TGF-b1 for cartilage tissue engineering. Macromol Biosci 9(12):1194–1201
144. Zhong Q, Jin M (2009) Zein nanoparticles produced by liquid–liquid dispersion. Food Hydrocoll 23(8):2380–2387
145. Chen H, Zhong Q (2015) A novel method of preparing stable zein nanoparticle dispersions for encapsulation of peppermint oil. Food Hydrocoll 43:593–602
146. Ghazy OA, Nabih S, Abdel-Moneam YK, Senna MM (2015) Synthesis and characterization of silver/zein nanocomposites and their application. Polym Composite 38(S1):E9–E15
147. Dhandayuthapani B, Poulose AC, Nagaoka Y, Hasumura T, Yoshida Y, Maekawa T, Kumar DS (2012) Biomimetic smart nanocomposite: in vitro biological evaluation of zein electrospun fluorescent nanofiber encapsulated CdS quantum dots. Biofabrication 4(2): 025008
148. Consonni R, Zetta L, Longhi R, Toma L, Zanaboni G, Tenni R (2000) Conformational analysis and stability of collagen peptides by CD and by 1H-and 13C-NMR spectroscopies. Biopolymers 53(1):99–111
149. Xu Y, Keene DR, Bujnicki JM, Höök M, Lukomski S (2002) Streptococcal Scl1 and Scl2 proteins form collagen-like triple helices. J Biol Chem 277(30):27312–27318
150. Ahsan SM, Mohan Rao Ch (2016) Structural studies on aqueous gelatin solutions: implications in designing a thermo-responsive nanoparticulate formulation. Int J Biol Macromol 95:1126–1134
151. Muralidharan N, Shakila RJ, Sukumar D, Jeyasekaran G (2013) Skin, bone and muscle collagen extraction from the trash fish, leather jacket (*Odonus niger*) and their characterization. J Food Sci Technol 50(6):1106–1113
152. Abdel-Mohsen AM, Jancar J, Abdel-Rahman RM, Vojtek L, Hyršl P, Dušková M, Nejezchlebová H (2017) A novel in situ silver/hyaluronan bio-nanocomposite fabrics for wound and chronic ulcer dressing: in vitro and in vivo evaluations. Int J Pharm 520(1–2): 241–253
153. Zhang L, Ma D, Wang F, Zhang Q (2002) The modification of scaffold material in building artificial dermis. Artif Cells Blood Substit Biotechnol 30(4):319–332
154. Mizuno K, Hayashi T, Peyton DH, Bächinger HP (2004) Hydroxylation-induced stabilization of the collagen triple helix acetyl-(glycyl-4 (r)-hydroxyprolyl-4 (r)-hydroxyprolyl) 10-nh2 forms a highly stable triple helix. J Biol Chem 279(36):38072–38078
155. Tampieri A, Celotti G, Landi E, Sandri M, Roveri N, Falini G (2003) Biologically inspired synthesis of bone-like composite: self-assembled collagen fibers/hydroxyapatite nanocrystals. J Biomed Mater Res Part A 67(2):618–625
156. Kumar P, Sandeep KP, Alavi S, Truong VD, Gorga RE (2010) Preparation and characterization of bio-nanocomposite films based on soy protein isolate and montmorillonite using melt extrusion. J Food Eng 100(3):480–489
157. Hassenkam T, Fantner GE, Cutroni JA, Weaver JC, Morse DE, Hansma PK (2004) High-resolution AFM imaging of intact and fractured trabecular bone. Bone 35(1), 4–10
158. Zhang J, Senger B, Vautier D, Picart C, Schaaf P, Voegel JC, Lavalle P (2005) Natural polyelectrolyte films based on layer-by layer deposition of collagen and hyaluronic acid. Biomaterials 26(16):3353–3361
159. Song L, Wang Z, Lamm ME, Yuan L, Tang C (2017) Supramolecular polymer nanocomposites derived from plant oils and cellulose nanocrystals. Macromolecules 50 (19):7475–7483
160. Saengruengrit C, Ritprajak P, Wanichwecharungruang S, Sharma A, Salvan G, Zahn DR, Insin N (2018) The combined magnetic field and iron oxide-PLGA composite particles: effective protein antigen delivery and immune stimulation in dendritic cells. J Colloid Interface Sci 520:101–111
161. Lu Y, Chen Y-C, Zhang P-H (2016) Preparation and characterisation of polylactic acid (PLA)/polycaprolactone (PCL) composite microfbre membranes. Fibres Text East Eur 3(117):17–21

162. Carson L, Kelly-Brown C, Stewart M, Oki A, Regisford G, Luo Z, Bakhmutov VI (2009) Synthesis and characterization of chitosan–carbon nanotube composites. Mater Lett 63(6–7): 617–620
163. Chiu HT, Chen SC (2001) Curing reaction of unsaturated polyester resin modified by dicyclopentadiene. J Polym Res 8(3):183–190
164. Hazarika D, Karak N (2016) Biodegradable tough waterborne hyperbranched polyester/carbon dot nanocomposite: approach towards an eco-friendly material. Green Chem 18(19): 5200–5211
165. Atila Dinçer C, Yildiz N, Karakeçili A, Aydoğan N, Çalimli A (2017) Synthesis and characterization of Fe_3O_4-MPTMS-PLGA nanocomposites for anticancer drug loading and release studies. Artif Cells Nanomed Biotechnol 45(7):1408–1414